



GluN3-Containing NMDA Receptors in the Rat Nucleus Accumbens Core Contribute to Incubation of Cocaine Craving

Daniel T. Christian,¹ Michael T. Stefanik,¹ Linda A. Bean,² Jessica A. Loweth,¹ Amanda M. Wunsch,¹ Jonathan R. Funke,¹ Clark A. Briggs,¹  Joseph Lyons,¹ Demetria Neal,² Mike Milovanovic,¹ Gary X. D'Souza,² Grace E. Stutzmann,¹ Daniel A. Nicholson,² Kuei Y. Tseng,¹ and  Marina E. Wolf¹

¹Rosalind Franklin University of Medicine and Science, North Chicago, Illinois 60064, and ²Rush University, Chicago, Illinois 60612

Cue-induced cocaine craving progressively intensifies (incubates) after withdrawal from cocaine self-administration in rats and humans. In rats, the expression of incubation ultimately depends on Ca²⁺-permeable AMPARs that accumulate in synapses onto medium spiny neurons (MSNs) in the NAc core. However, the delay in their accumulation (~1 month after drug self-administration ceases) suggests earlier waves of plasticity. This prompted us to conduct the first study of NMDAR transmission in NAc core during incubation, focusing on the GluN3 subunit, which confers atypical properties when incorporated into NMDARs, including insensitivity to Mg²⁺ block and Ca²⁺ impermeability. Whole-cell patch-clamp recordings were conducted in MSNs of adult male rats 1–68 d after discontinuing extended-access saline or cocaine self-administration. NMDAR transmission was enhanced after 5 d of cocaine withdrawal, and this persisted for at least 68 d of withdrawal. The earliest functional alterations were mediated through increased contributions of GluN2B-containing NMDARs, followed by increased contributions of GluN3-containing NMDARs. As predicted by GluN3-NMDAR incorporation, fewer MSN spines exhibited NMDAR-mediated Ca²⁺ entry. GluN3A knockdown in NAc core was sufficient to prevent incubation of craving, consistent with biotinylation studies showing increased GluN3A surface expression, although array tomography studies suggested that adaptations involving GluN3B also occur. Collectively, our data show that a complex cascade of NMDAR and AMPAR plasticity occurs in NAc core, potentially through a homeostatic mechanism, leading to persistent increases in cocaine cue reactivity and relapse vulnerability. This is a remarkable example of experience-dependent glutamatergic plasticity evolving over a protracted window in the adult brain.

Key words: calcium-permeable AMPAR; GluN3; incubation of cocaine craving; medium spiny neuron; NMDAR; NAc core

Significance Statement

“Incubation of craving” is an animal model for the persistence of vulnerability to cue-induced relapse after prolonged drug abstinence. Incubation also occurs in human drug users. AMPAR plasticity in medium spiny neurons (MSNs) of the NAc core is critical for incubation of cocaine craving but occurs only after a delay. Here we found that AMPAR plasticity is preceded by NMDAR plasticity that is essential for incubation and involves GluN3, an atypical NMDAR subunit that markedly alters NMDAR transmission. Together with AMPAR plasticity, this represents profound remodeling of excitatory synaptic transmission onto MSNs. Given the importance of MSNs for translating motivation into action, this plasticity may explain, at least in part, the profound shifts in motivated behavior that characterize addiction.

Received Feb. 24, 2021; revised Aug. 6, 2021; accepted Aug. 10, 2021.

Author contributions: D.T.C., G.E.S., D.A.N., K.Y.T., and M.E.W. designed research; D.T.C., M.T.S., L.A.B., J.A.L., A.M.W., J.R.F., C.A.B., J.L., D.N., M.M., G.X.D., and D.A.N. performed research; D.T.C., M.T.S., L.A.B., J.A.L., A.M.W., J.L., D.N., G.X.D., G.E.S., D.A.N., K.Y.T., and M.E.W. analyzed data; D.T.C., K.Y.T., and M.E.W. wrote the first draft of the paper; D.T.C., M.T.S., L.A.B., J.A.L., A.M.W., J.R.F., C.A.B., J.L., D.N., M.M., G.X.D., G.E.S., D.A.N., K.Y.T., and M.E.W. edited the paper; D.T.C., K.Y.T., and M.E.W. wrote the paper.

This work was supported by National Institute on Drug Abuse Grants R01 DA015835 to M.E.W., F32 DA036963 to D.T.C., F32 DA040414 to M.T.S., K99-R00 DA038110 to J.A.L., F32 DA046141 to A.M.W., and AG017139 to D.A.N.

D.T. Christian's present address: Department of Physiology and Pharmacology, Des Moines University, Des Moines, IA 50312.

M.T. Stefanik's present address: Department of Psychology and Neuroscience, North Central College, Naperville, IL 60540.

L.A. Bean's present address: Department Neuroscience, McKnight Brain Institute, University of Florida, Gainesville, FL 32611.

A.M. Wunsch's, J.R. Funke's, and M.E. Wolf's present address: Department of Behavioral Neuroscience, Oregon Health & Science University, Portland, OR 97212.

K.Y. Tseng's present address: Department of Anatomy and Cell Biology, University of Illinois at Chicago, Chicago, IL 60612.

The authors declare no competing financial interests.

Correspondence should be addressed to Marina E. Wolf at wolfmar@ohsu.edu.

<https://doi.org/10.1523/JNEUROSCI.0406-21.2021>

Copyright © 2021 the authors

Introduction

Cue-induced craving for cocaine and other drugs of abuse progressively intensifies (“incubates”) in rodents after withdrawal from extended-access drug self-administration (Pickens et al., 2011). Incubation of craving also occurs in human drug users during forced abstinence, arguing that the rodent model is valuable for understanding the persistence of vulnerability to relapse, a major challenge in overcoming addiction (Li et al., 2016). Although many brain regions contribute to incubation, medium spiny neurons (MSNs) in the core subregion of the NAc play a critical role once cocaine craving has plateaued (Hollander and Carelli, 2005, 2007; Guillem et al., 2014; Wolf, 2016). Heightened activation of NAc MSNs, attributable to synaptic incorporation of high conductance GluA2-lacking, Ca²⁺-permeable AMPARs (CP-AMPARs), is required for the expression of incubated cocaine craving in late withdrawal in response to presentation of cues previously paired with cocaine (Conrad et al., 2008; Loweth et al., 2014).

Interestingly, CP-AMPA plasticity has a slower onset than incubation of cue-induced drug seeking itself. A significant increase in cue-induced seeking is evident even during the first week of cocaine withdrawal (Grimm et al., 2001). In contrast, using the characteristic property of inward rectification to assess the contribution of CP-AMPA-mediated synaptic currents in the NAc core after extended-access cocaine self-administration, we observed no change in the rectification index over the first 3 weeks of withdrawal, a trend toward an increase around withdrawal day (WD) 25, and a statistically significant increase by WD30–WD35 that was then maintained through at least WD70 (Wolf and Tseng, 2012). Biochemical evidence of increased homomeric GluA1 receptors was first detected on WD21 (Conrad et al., 2008). The delay in CP-AMPA accumulation in the NAc core suggests a requirement for earlier waves of plasticity. Here we investigated the possibility of earlier plasticity involving NMDAR transmission.

NMDARs are tetramers containing two copies of the obligatory GluN1 subunit plus GluN2 subunits (GluN2A–D) and/or GluN3 subunits (GluN3A or GluN3B). They may be diheteromeric receptors (e.g., GluN1/GluN2B) or triheteromeric receptors containing two different GluN2 subunits or a combination of GluN2 and GluN3 subunits (Dunah and Standaert, 2003; Hansen et al., 2018; Stroebel et al., 2018). Typically, GluN3 inclusion endows NMDARs with lower conductance, reduced Ca²⁺ permeability, and insensitivity to Mg²⁺ block (Pachernegg et al., 2012; Perez-Otano et al., 2016). Of particular interest is the association between GluN3 and addiction-related phenotypes (Chen et al., 2018).

In preclinical studies, increased GluN3 levels contribute to alter corticostriatal plasticity after methamphetamine self-administration (X. Huang et al., 2017). In VTA dopamine neurons, acute cocaine injection leads to synaptic incorporation of both GluN3-containing NMDARs (GluN3-NMDARs) and CP-AMPARs (Mameli et al., 2011; Yuan et al., 2013; Creed et al., 2016), which in turn shifts the rules for induction of LTP (Mameli et al., 2011). Normally, NMDARs serve as coincidence detectors for Hebbian plasticity, but GluN3-NMDARs cannot fulfill this role because of their decreased Ca²⁺ permeability and Mg²⁺ sensitivity. CP-AMPARs provide an alternate Ca²⁺ source that enables Ca²⁺ entry at hyperpolarized potentials. Thus, cocaine-induced incorporation of both GluN3-NMDARs and CP-AMPARs in dopamine neurons favors LTP induction when presynaptic release occurs together with postsynaptic hyperpolarization (Mameli et al.,

2011). This, in turn, predicts substantial alterations for subsequent synaptic plasticity and reward learning. These results led us to wonder whether GluN3-NMDARs might be contributing, along with CP-AMPARs, to synaptic plasticity in the NAc core during incubation of cocaine craving.

In the striatum and NAc, GluN3B is moderately expressed and localized to both MSNs and interneurons (Wee et al., 2008), whereas GluN3A levels are lower (Wong et al., 2002). The functional roles of GluN3 subunits in the NAc core have not been explored. Here we used slice physiology, spine-level imaging, biochemistry, and behavioral analyses to demonstrate time-dependent NMDAR plasticity involving GluN2B and GluN3 subunits in NAc core MSNs that precedes CP-AMPA accumulation and is required for incubation of cocaine craving.

Materials and Methods

Subjects and surgery. All experimental procedures were approved by the Rosalind Franklin University Institutional Animal Care and Use Committee in accordance with the US Public Health Service Guide for Care and Use of Laboratory Animals. Adult male Sprague Dawley rats (250–275 g on arrival) were group housed on a reverse 12 h light/dark cycle. They were acclimated to the animal facility for ~7 d before undergoing surgery for intravenous catheter implantation as described previously (Conrad et al., 2008; Loweth et al., 2014). Briefly, rats were anesthetized via injection of a ketamine-xylazine cocktail (80–10 mg/kg i.p., respectively). A Silastic catheter (Plastics One) was inserted into the right jugular vein and passed subcutaneously to the mid-scapular region. Animals were administered Banamine (MWI Animal Health) for post-surgical analgesia and allowed to recover under single housing conditions for ~7 d. During recovery and self-administration training, catheters were flushed every 24–48 h with cefazolin (15 mg, IV Webster Veterinary Supply) in sterile saline. Groups of animals assigned to experiments involving viral knockdown of GluN2B or GluN3A subunits underwent virus infusion ~4 weeks before catheter surgery (see below).

Cocaine self-administration training and tests for cue-induced cocaine seeking. Rats were trained to self-administer cocaine or saline (control condition) using a fixed-ratio 1 reinforcement schedule during daily 6 h sessions for 10 d (Conrad et al., 2008; Loweth et al., 2014). Cocaine hydrochloride (from National Institute on Drug Abuse) was dissolved in saline (0.5 mg/kg/infusion in a 100 μ l/kg volume over 3 s). Self-administration sessions occurred during the dark cycle in operant chambers (Med Associates) equipped with two nose-poke holes. Responses in the active hole activated an infusion pump paired with the delivery of a 20 s light cue inside the active hole. Each infusion was followed by a 20 s timeout period when behavioral responses were recorded but not rewarded. Behavioral responses in the inactive hole were recorded but had no consequence. Rats were killed if they did not learn to self-administer cocaine and/or had a faulty catheter. Following the last self-administration session, animals were placed back into their home cages where they underwent withdrawal/forced abstinence (these terms are used interchangeably to indicate cessation of drug availability). During the withdrawal period, some groups of animals underwent cue-induced seeking tests. Rats were returned to operant chambers on the specified WD and tested for 30 min under extinction conditions; that is, nose-pokes in the active hole resulted in presentations of the light cue previously paired with cocaine infusions, but no cocaine. The number of responses in the previously active hole was our operational measure of cocaine seeking or craving. For experiments involving acute infusion of 4-(2,4-dichlorobenzoyl)-1H-pyrrole-2-carboxylic acid (TK30) before seeking tests, rats received surgical implantation of bilateral guide cannulae directed at the NAc core after ~3 weeks of cocaine withdrawal (~2 weeks before the first of two cue-induced seeking tests) using coordinates and procedures described previously (Werner et al., 2018).

Adeno-associated virus (AAV) construction, infusion, and behavioral testing. For GluN2B experiments, we used an AAV2 packaged RNAi to GluN2B (GCTGGTGATAATCCTTCTGAA) or a luciferase control RNAi (CCTAAGGTTAAGTCGCCCTCG) described previously (J.

Wang et al., 2018) and provided by Drs. Yan Dong and Oliver Schlüter (University of Pittsburgh). GluN3A knockdown was achieved using AAV5-CMV-EGFP-H1-shNR3A1185 (CTACAGCTGAGTTTAGAAA) along with a scrambled control virus AAV5-GFP-U6-scrmb-shRNA (CAACAAGATGAAGACACCAA), prepared by Vector Biolabs, based on information for viruses previously used by Camilla Bellone and colleagues (Yuan et al., 2013). Virus injection into the NAc core occurred ~4 weeks before catheter implantation (i.e., 5 weeks before start of drug self-administration), allowing for robust expression of the viral construct before the onset of drug withdrawal. Rats received stereotaxic injections of virus (0.5 μ l per side) into the NAc core over 5 min. Injectors were left in place for 5 min. Catheter surgery and drug self-administration training were subsequently performed as described above. Rats were tested for cue-induced cocaine seeking on WD1, to obtain a measure of baseline seeking, and again after protracted withdrawal (WD44-WD49).

Electrophysiology. Whole-cell patch-clamp recordings were performed as described previously (Conrad et al., 2008; McCutcheon et al., 2011; Loweth et al., 2014). Briefly, rats were anesthetized using chloral hydrate (400–600 g/kg, i.p.), brains were rapidly removed, and coronal slices at the level of the NAc (350 μ m) were cut with a vibrating microtome in ice-cold sucrose-based cutting solution. They were transferred to warm (32°C–34°C) aCSF containing the following (in mM): 122.5 NaCl, 20 glucose, 25 NaHCO₃, 2.5 KCl, 0.5 CaCl₂, 3 MgCl₂, 1.0 NaH₂PO₄, 1.0 ascorbic acid. All recordings were conducted at least 1 h after slicing. All solutions were constantly oxygenated (95% O₂/5% CO₂). Whole-cell patch-clamp recordings were conducted in room temperature aCSF with CaCl₂ increased to 2.5 mM and MgCl₂ reduced to 1.0 mM. Picrotoxin (0.1 mM) and CNQX (0.02 mM) were used to block GABAergic and AMPAR-mediated synaptic transmission, respectively, enabling us to isolate NMDAR-mediated currents. This was confirmed using the NMDAR antagonist DL-2-amino-5-phosphonopentanoic acid sodium salt (APV, 0.05 mM; data not shown). Patch pipettes (6–8 M Ω) were filled with internal solution containing the following (in mM): 140 CsCl, 10 HEPES, 2 MgCl₂, 5 NaATP, 0.6 NaGTP, 2 QX-314, 0.1 spermine. NAc MSNs from the core region were identified under visual guidance using infrared-differential interference contrast video microscopy with a 40 \times water immersion objective (Olympus BX51-WI). The image was detected with an infrared-sensitive CCD camera and displayed on a monitor. Whole-cell patch-clamp recordings were performed with a computer-controlled amplifier (Axoclamp200B; Molecular Devices), digitized (Digidata 1322a; Molecular Devices), and acquired for later analysis with pClamp 10 (Molecular Devices) at a sampling rate of 10 kHz. The liquid junction potential was not corrected, and electrode potentials were adjusted to zero before obtaining the whole-cell configuration. Glutamatergic NAc MSN synaptic responses were elicited by local electrical stimulation (0.2 ms duration) delivered every 20 s using concentric bipolar stimulating electrodes (FHC). Importantly, stimulation intensities were adjusted between cells to levels that resulted in a ~50 pA response at –20 mV from the reversal potential (for rationale, see first paragraph of Results). *I*–*V* responses were collected relative to the reversal potential at –80, –40, 0 mV (reversal potential), and 40 mV (also used for measures of decay kinetics) and analyzed using Clampfit10 (Molecular Devices) and GraphPad Prism. Components of aCSF and internal solutions, as well as picrotoxin, were purchased from Sigma-Aldrich. CNQX was purchased from Alomone Labs. (1R*,2S*)-erythro-2-(4-benzylpiperidino)-1-(4-hydroxyphenyl)-1-propanolhemi-(DL)-tartrate (ifenprodil) and (R)- α -methylamino-2,3-dihydro-4-methoxy-7-nitro- γ -oxo-1H-indole-1-butanoic acid (MNI-caged-NMDA) were purchased from Tocris. TK30 was purchased from Key Organics. DL-APV was purchased from Abcam.

Analysis of surface-expressed and total NMDAR subunits. Rats self-administered saline or cocaine as described above and were killed after 2, 14, 25, or 48 d of withdrawal. These groups were run between 2011 and 2013. Bilateral NAc tissue (mainly core subregion) was punched from coronal slices prepared with a brain matrix, and NAc tissue was biotinylated as detailed previously (Ferrario et al., 2011b; Loweth et al., 2014); and then frozen at –80°C. In 2013, an aliquot of biotinylated starting material (total protein) was retained for each rat, and the remaining biotinylated NAc sample was processed to separate biotinylated proteins bound to NeutrAvidin beads (bound material, surface-

expressed proteins) from the nonbiotinylated (unbound) material. Total protein and bound material were analyzed by immunoblotting in 2013 and 2014, as described under Western analysis. Self-administration data for these rats were published previously as part of a study that used aliquots of their NAc tissue to study the role of Group 1 metabotropic glutamate receptors and Homer proteins in the incubation of cocaine craving (Loweth et al., 2014). Other aliquots were used to study expression of hypocretin receptors (Plaza-Zabala et al., 2013) and GABA_A receptors (Purgianto et al., 2016). Although immunoblotting for NMDAR subunits was completed in 2014, as noted above, the data were not published at that time because we were undertaking additional experiments (e.g., electrophysiology, calcium imaging, array tomography, and viral knockdowns) now presented in the current study.

Analysis of NMDAR subunits in postsynaptic density (PSD) fractions. Male rats self-administered saline or cocaine as described above and were killed after either 5 or 40 d of withdrawal in 2017, with tissue processing and immunoblotting completed within weeks of obtaining samples. Briefly, bilateral NAc tissue (mainly core subregion) was punched from slices prepared with a brain matrix. To obtain a Triton-insoluble PSD fraction, we used a previously described subcellular fractionation procedure (Davies et al., 2007, 2008; Goebel-Goody et al., 2009) that we have validated in our laboratory (Ferrario et al., 2011a). Each NAc sample was homogenized in 3 ml of sucrose homogenization buffer (10 mM HEPES, 0.32 M sucrose, 5 mM NaF, 1 mM NaVO, 2 mM EDTA, pH 7.4) in a glass grinding vessel with a rotating Teflon pestle (Wheaton Overhead Stirrer; 3000 RPM for 12 passes). The homogenate was centrifuged (800 \times g, 10 min, 4°C) to remove the pelleted nuclear fraction (P1). The resulting supernatant (S1) was centrifuged (10,000 \times g, 15 min, 4°C) to yield a crude membrane fraction (P2). The P2 fraction was washed twice with sucrose homogenization buffer and resuspended in 4 ml of HEPES-buffered sucrose containing 0.5% Triton X-100 (0.5% v/v) using a motorized pellet pestle mixing/grinding rod (Kontes). The suspension was then incubated with gentle rotation (20 min, 4°C) and centrifuged (32,000 \times g, 20 min) to yield the insoluble pellet (PSD fraction), which was washed twice before use. The PSD fraction was resuspended in Laemmli sample treatment buffer containing 100 mM DTT. Samples were then stored at –80°C.

Western analysis. Samples were heated at 95°C for 3 min in Laemmli sample treatment buffer with 100 mM DTT and then processed for SDS-PAGE and immunoblotting as described previously for total and cell surface analysis (Ferrario et al., 2010, 2011b; Loweth et al., 2014). For PSD analysis, samples were run on 4%–12% Bis-Tris gels (Bio-Rad) and transferred to PVDF membranes (Murray et al., 2019, 2021). For all immunoblotting, membranes were incubated in blocking solution (5% evaporated milk, 1% normal goat serum in TBS-T) for 1 h at room temperature and incubated in primary antibody diluted in TBS-T overnight at 4°C. Membranes were washed in TBS-T solution, incubated at room temperature for 60 min with either goat anti-rabbit IgG (H + L) (1:10,000, Invitrogen, G21234) or goat anti-mouse IgG (H + L) (1:10,000, Invitrogen, G21040), washed with TBS-T, and then immersed in chemiluminescence detecting substrate (GE Healthcare). Images of immunoblots were taken using a GE HealthcareImager 600 (GE Healthcare) and quantified using ImageQuant TL software (GE Healthcare). Background values were obtained, and diffuse densities for bands of interest in each lane were determined. For starting material (total protein) and the biotinylated fraction (surface protein), loading was determined by a protein assay. For starting material samples only, data for each protein of interest were normalized to total protein in each lane determined by Ponceau S staining. This correction was not performed for the biotinylated fraction, as we have found that Ponceau S staining is unreliable in the bound (surface) fraction (e.g., Loweth et al., 2014; Murray et al., 2021). Because the PSD samples are solubilized directly in SDS, measures of protein concentration in the PSD fraction are unreliable. Therefore, PSD samples were loaded according to volume, as we have done previously (Ferrario et al., 2011b). For all samples, data are presented as mean \pm SEM expressed as percent of control. For some proteins, we were unable to quantify immunoreactivity for some lanes because of an unclear band, smudge on the blot, or air bubble

obstructing the signal. Therefore, the n value for Western blotting data (provided in the figure legends) may vary from the total number of rats treated. The following primary antibodies were used for analysis of biotinylation experiments (starting material and biotinylated fraction), with studies validating antibody specificity listed in parentheses after each antibody: GluN1 (1:100), mouse, Novus Biologicals, NB300-118 (Garraway et al., 2009); GluN2A (1:2000), goat, Santa Cruz Biotechnology, SC-1468 (Tezuka et al., 1999); GluN2B (1:2500), rabbit, Calbiochem, 454582 (Snell et al., 1996; Curras and Dao, 1998; Khan et al., 1999); GluN3A (1:1000), rabbit, Millipore, 07-356 (Wee et al., 2008); and GluN3B (1:250), rabbit, Millipore, 07-351 (Wee et al., 2008). The following primary antibodies were used for analysis of PSD fractions, with studies validating antibody specificity listed in parentheses after each antibody: GluN1 (1:500) rabbit, Cell Signaling Technology, 5704 (Y. Wang et al., 2015) and Cell Signaling Technology Product Information; GluN2A (1:1000), rabbit, Novus Biologicals, NB300-105 (Novus Product Datasheet, version 20.1, updated September 14, 2016); GluN2B (1:1000), rabbit, Cell Signaling Technology, 14544 (Pietrogrande et al., 2019; Yang et al., 2020); GluN3A (1:200), rabbit, OriGene, TA328843 (OriGene Product Information); and GluN3B (1:200), rabbit, OriGene, TA328844 (OriGene Product Information).

2-Photon Ca^{2+} imaging. Ca^{2+} imaging studies were conducted similarly to our previous reports (Stutzmann et al., 2003; Ferrario et al., 2012; Briggs et al., 2013). A custom-designed video rate multiphoton system based on an upright Olympus BX51 frame was used to image fura-2 Ca^{2+} -fluorescence signals within MSNs. Laser excitation from a Ti:Sapphire laser (Mai Tai Broadband, Spectra-Physics) was provided by trains of ~ 100 fs pulses (80 MHz) at 780 nm. A resonant galvanometer (General Scanning Lumonics) scanned the laser beam allowing rapid (7.9 kHz) bidirectional scanning in the x axis, while a conventional linear galvanometer scanned in the y axis to provide full frame scan of 30 fps. A $40\times$ water-immersion objective (NA = 0.8) was used to focus the laser onto the tissue sample, and emitted fluorescence was detected by a wide-field photomultiplier (Electron Tubes) to derive video signals captured and analyzed by Video Savant 4.0 software (IO Industries). Analysis of background-corrected images was conducted using MetaMorph 7.0 software (Molecular Devices). Pseudocolored images of fura-2 fluorescence are expressed as inverse pseudo-ratios such that increases in $[Ca^{2+}]$ correspond to increasing ratios of $F_0/\Delta F$ (F_0 is the average resting fluorescence at baseline, and ΔF is the decrease of fluorescence on Ca^{2+} release). Data indicating relative percentage changes in fluorescent intensity were calculated as percent over baseline: $(F_0/\Delta F - 1) \times 100$. UV flash photolysis of caged compounds was accomplished using an X-Cite 120 Fluorescence Illumination system (Photonic Solution) and a narrow UV filter cube (360–380 nm) in a light path separate from the laser input, with exposure time determined by electronic shutters (Uniblitz, Vincent Associates) operated and synchronized through digital outputs (Digidata 1322 A-D board) controlled by pClamp 10.2. The percentage of spine heads generating an NMDAR-mediated Ca^{2+} response within a full image frame was determined by counting the total number of visible spines and determining the fraction of “responding” spines, expressed as “% responding.” The threshold for Ca^{2+} responding was determined by a signal temporally synchronized with the UV flash at least 10% over baseline level with onset and decay kinetics distinguishable from background. Groups were compared with a two-tailed t test (significance set at $p < 0.05$). Experiments were performed in the presence of cadmium (100 μM), applied in circulating aCSF 10 min before the start of baseline imaging, to eliminate contributions of voltage-gated Ca^{2+} channels. MNI-caged NMDA (Palma-Cerda et al., 2012) was bath applied for 2.5 min before photo-uncaging.

Array tomography. Immunofluorescence array tomography was used to visualize the dendrites of biocytin-filled neurons and probe for the molecular markers of interest, as in our prior studies (e.g., Neuman et al., 2015). Slices were postfixed in 4% PFA for 3–7 d immediately following patch-clamp experiments. Slices were washed in PBS, permeabilized, and bathed in 1:200 dilution of streptavidin-conjugated AlexaFluor-488 (Invitrogen) for 48 h at 4°C. Slices were trimmed to include only the filled neuron, fixed and dehydrated with microwave processing (Pelco BioWave Pro), embedded in LR White resin (Electron Microscopy Sciences), and

cured at 52°C for 20 h. Cured blocks were hand trimmed to a rectangle containing the immunostained neuron. Arrays of 50–150 serial ultrathin sections (70 nm) were collected using an ultramicrotome (Leica Microsystems UC6) with a jumbo histo diamond knife (Diatome), mounted onto coverslips (Aratome), and dried. Arrays were blocked, immunostained with primary antibody overnight at 4°C, rinsed with TBS, incubated in secondary antibodies for 30 min at room temperature, rinsed with TBS, and mounted with SlowFade Diamond AntiFade with DAPI (Invitrogen). Images were acquired with a Carl Zeiss AxioImager.M2 system equipped with an Axiocam MRm digital camera, AxioVision Software, and $63\times/1.4$ NA Plan Apochromat oil-immersion objective lens, and mosaics were obtained with the aid of custom-written plugins provided by Stephen Smith's laboratory. Immediately following imaging of the array, the antibodies were eluted, the coverslip was washed, dried, and prepared for another session of staining. Imaged arrays from multiple sessions were stitched, stacked, aligned, and cropped using ImageJ software. Stacks were deconvolved using AxioVision Software. 3D images were rendered and analyzed using Imaris by Bitplane. The following primary antibodies were used: GluA1 (1:50), rabbit, Cell Signaling, AB1504; GluA2 (1:50), mouse, Millipore, MAB397; GluN1 (1:50), mouse, Millipore, MAB363; GluN2B (1:100), rabbit, Sigma, SAB4300425; GluN3A (1:100), rabbit, Millipore, 07-356; GluN3B (1:50), rabbit, Millipore, 07-351; and PSD95 (1:50), goat, Abcam, AB12093. The following secondary antibodies were used: Alexa-594, donkey, Invitrogen, A21207; Alexa-647, donkey, Invitrogen, A31571; and Alexa-647, donkey, Invitrogen, A21447. Antibodies were validated via Western blot on mouse tissue to ensure that the antibody recognized a single band at the approximate, appropriate molecular weight for each epitope; furthermore, each new batch of antibody was tested in two separate immunostaining sessions on rat tissue, and puncta were required to have $>85\%$ concordance on the same tissue (test-retest rate of $\geq 85\%$). That is, the same puncta were required to be either negative or positive for $>85\%$ of the pixels. Furthermore, antibodies were not used if immunofluorescence signal was present in the nucleus.

Experimental design and statistical analyses. Rats destined for electrophysiological recordings self-administered saline or cocaine and were killed at withdrawal times ranging from 1 to 68 d for preparation of brain slices (all methods described above). A total of 133 male rats were used. Each electrophysiological endpoint was evaluated in a minimum of 5 cells from 3 different rats; data are expressed as mean \pm SEM. Student's t tests (paired/unpaired as noted in text) were used to compare two groups. To compare >2 groups, we used ANOVA followed by Holm-Sidak *post hoc* tests. Details of statistical design and outcomes for these electrophysiological studies are presented in the legends to Figures 1–4. To determine whether incubation of craving is associated with altered Ca^{2+} entry into MSN spines, male rats self-administered saline or cocaine and brain slices were prepared after WD39 for 2-photon Ca^{2+} imaging (all methods described above). We imaged 122 spines (10 cells; 4 rats) for the cocaine group and 135 spines (10 cells; 5 rats) for the saline group. Details of statistical design and outcomes for these 2-photon Ca^{2+} imaging can be found in the legend to Figure 5. To measure surface-expressed and total NMDAR subunits levels, male rats self-administered saline or cocaine, and the NAc (mainly core) was dissected on WD2, WD14, WD25, or WD48, time points selected to bracket the emergence of CP-AMPA in the NAc core (see Introduction). Tissue was biotinylated, the biotinylated surface-expressed proteins were isolated, and samples were analyzed by immunoblotting as described above. An aliquot of starting material or biotinylated/surface fraction from the NAc of a single rat was loaded into each lane of the gels. After eliminating lanes that could not be analyzed, the biotinylated/surface fraction of each subunit was analyzed in 9–11 saline rats and 10–12 cocaine rats for WD2, 10 or 11 saline rats and 11 cocaine rats for WD14, 7–10 saline rats and 9–11 cocaine rats for WD25, and 6–8 saline rats and 6–11 cocaine rats for WD48. Ranges are given for n values because n depends on the subunit measured; each subunit was analyzed on separate gels, and gels differed as to whether any lanes could not be analyzed. For starting material, at least as many samples were analyzed for each subunit/experimental group. Saline and cocaine groups were compared using a

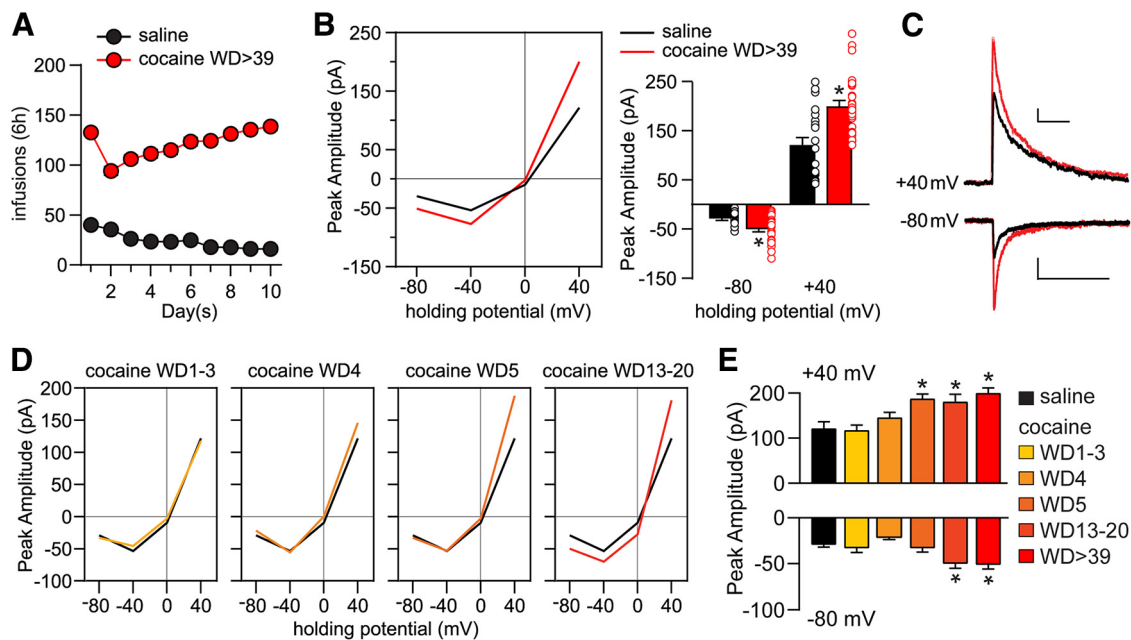


Figure 1. Time-dependent regulation of NMDAR-mediated synaptic transmission in NAc core MSNs during withdrawal from extended-access cocaine self-administration. **A**, Training data for rats used in electrophysiological experiments. Male rats self-administered saline ($n = 41$) or cocaine ($n = 92$) 6 h/day for 10 consecutive days. **B**, Whole-cell patch-clamp recordings of NMDAR-mediated EPSCs were performed in NAc core MSNs of saline rats (23 cells/15 rats) on or after WD 16 and from cocaine rats (29 cells/22 rats) between WD39 and WD68. These saline and/or cocaine data are reproduced for comparative purposes in Figures 2–4. Left, I – V plot of response amplitudes at different membrane holding potentials. Right, Summary data at 40 mV and -80 mV holding potentials (individual data points and mean \pm SEM are shown). Cocaine cells exhibit increased response amplitudes at -80 and 40 mV compared with saline cells. -80 mV: saline versus cocaine, unpaired t test, $t_{(50)} = 3.58$, $p = 0.0008$; 40 mV: saline versus cocaine, unpaired t test, $t_{(50)} = 4.394$, $p < 0.0001$; $*p < 0.05$. **C**, Representative traces of saline (black) and cocaine WD > 39 (red) cells at 40 mV and -80 mV. Calibration: 40 mV: 50 pA \times 250 ms; -80 mV: 20 pA \times 250 ms. **D**, I – V plots of NMDAR-mediated synaptic transmission of cocaine cells at different withdrawal time points: WD1–WD3 (15 cells/7 rats), WD4 (16 cells/8 rats), WD5 (11 cells/7 rats), and WD13–WD20 (15 cells/12 rats). **E**, Response amplitudes for saline and each cocaine withdrawal group. ANOVA was used to analyze data for each holding potential, with comparisons conducted using Holm–Sidak *post hoc* tests. 40 mV: $F_{(5,102)} = 7.918$, $p < 0.0001$; saline versus WD5, $p = 0.0226$; saline versus WD13–WD20, $p = 0.0266$; saline versus WD > 39 , $p < 0.0001$; WD1–WD3 versus WD5, $p = 0.0266$; WD1–WD3 versus WD13–WD20, $p = 0.0298$; WD1–WD3 versus WD > 39 , $p = 0.0002$; WD4 versus WD > 39 , $p = 0.0266$. -80 mV: $F_{(5,102)} = 7.670$, $p < 0.0001$; saline versus WD13–WD20, $p = 0.0178$; saline versus WD > 39 , $p = 0.001$; WD1–WD3 versus WD > 39 , $p = 0.0365$; WD4 versus WD13–WD20, $p = 0.001$; WD4 versus WD > 39 , $p < 0.0001$; $*p < 0.05$.

Student's t test at each WD time point. Details of statistical design and outcomes can be found in the legend to Figure 6. Because we observed an increase in surface GluN3A on WD48 in the biotinylation experiments described immediately above, we followed up by measuring NMDAR subunit levels in PSD fractions of the NAc core. Male rats self-administered saline or cocaine, and the NAc (mainly core) was dissected on WD5, when GluN2B plasticity has emerged (see Results), or WD40, when GluN3 and CP-AMPA plasticity is established (see Results and Introduction). PSD fractions were prepared and analyzed by immunoblotting. All methods are described above. An aliquot of PSD material from the NAc of a single rat was loaded into each lane of the gels. After eliminating lanes that could not be analyzed, each subunit was analyzed in 10 or 11 saline rats and 9 or 10 cocaine rats for WD5, and 8 or 9 saline rats and 6 or 7 cocaine rats for WD40 (see above for explanation of n value ranges). Data were analyzed using a Student's t test at each WD time point, saline versus cocaine. Details of statistical design and outcomes for these immunoblotting experiments can be found in the legend to Figure 7. For high-resolution analysis of NMDAR subunits in single NAc core spines, male rats self-administered saline or cocaine; after WD30, slices were processed for immunofluorescence array tomography. For the saline group, analysis was based on four cells, 12 dendrites, and 825 spines from 3 rats (WD > 38). For the cocaine group, analysis was based on four cells, 9 dendrites, 965 spines from 2 rats (WD46 and WD47); this group is named WD > 39 in Figure 8 to conform with late withdrawal groups in other figures. Details of statistical design and outcomes for these array tomography studies can be found in the legend to Figure 8. Further analysis of the array tomography data was performed to determine centrality versus laterality of glutamate receptor subunit localization relative to the PSD (defined by PSD95 staining). Details of statistical design and outcomes can be found in the legend to Figure 9. For GluN3A or GluN2B viral knockdown experiments, male rats

received intra-NAc infusion of viruses 5 weeks before the start of cocaine self-administration training and received cue-induced seeking tests on WD1 and in late withdrawal (all methods described above). Between 9 and 12 rats were infused with each virus. Data were analyzed with a three-way repeated-measures ANOVA (nose-poke hole \times virus condition \times WD), and the effect of viral manipulation on incubation was then probed using planned comparisons with a Bonferroni correction. For each target (GluN3A or GluN2B), two comparisons were made (cue-induced seeking on WD1 vs late withdrawal for control animals and cue-induced seeking on WD1 vs late withdrawal for active virus animals), so significance was set at $p < 0.025$. Additional information on statistical design and outcomes for these knockdown experiments can be found in the legends to Figure 10A–D (GluN3A) and Figure 11 (GluN2B). We did not quantify target knockdown in these animals because they were used to attempt electrophysiological analysis of the consequences of virus expression (these experiments were not successful). However, while cutting slices for recordings, virus expression and correct localization in the NAc core were confirmed for all animals included in the behavioral analyses. Finally, to determine whether expression of incubated craving requires activation of GluN3-NMDARs, male rats self-administered cocaine and received cue-induced seeking tests in late withdrawal. Vehicle or TK30 (30 μ M in 0.5 μ l/hemisphere) was infused bilaterally into the NAc core 1 h before the seeking test (a crossover design yielded 10 measures per group). Methods are described above. Data were analyzed with two-way ANOVA and Holm–Sidak tests. For all animals included in the analysis, virus expression in NAc core was confirmed histologically. Details of statistical design and outcomes for this experiment can be found in the legend to Figure 10E–G. For all experiments except the GluN3A and GluN2B knockdown experiments described above, significance was set at $p < 0.05$.

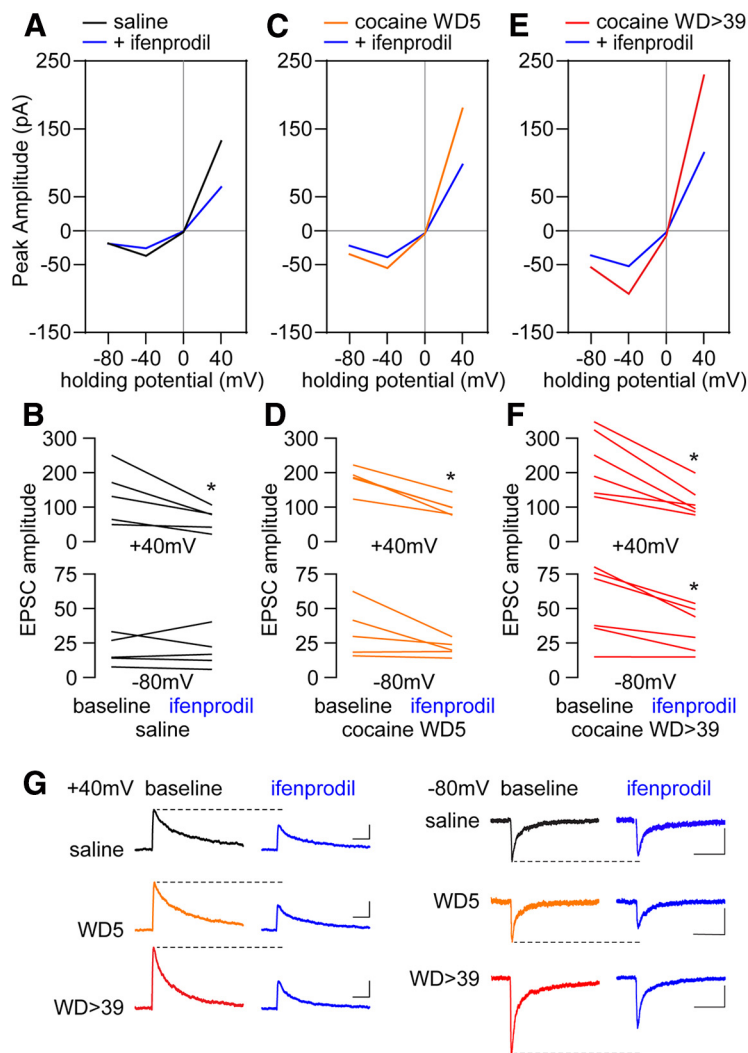


Figure 2. Ifenprodil, a GluN2B antagonist, reduces NMDAR-mediated EPSCs by the same relative degree in saline and cocaine groups. **A, B,** Within-cell application of ifenprodil ($5 \mu\text{M}$) to saline cells (5 cells/4 rats) significantly reduced response amplitudes at 40 mV (saline vs saline + ifenprodil, paired t test, $t_{(4)} = 2.88$, $p = 0.045$), but not -80 mV (saline vs saline + ifenprodil, paired t test, $t_{(4)} = 0.052$, $p = 0.9613$). These data suggest that GluN2B-containing NMDARs are present under control conditions but only contribute at depolarized membrane potentials. **C, D,** In cocaine WD5 cells (5 cells/3 rats), within-cell application of ifenprodil significantly reversed the increased amplitudes at 40 mV (cocaine WD5 vs cocaine WD5 + ifenprodil, paired t test, $t_{(4)} = 7.101$, $p = 0.0021$). A trend was observed at -80 mV (cocaine WD5 vs cocaine WD5 + ifenprodil, paired t test, $t_{(4)} = 1.921$, $p = 0.12$). **E, F,** In cocaine WD > 39 cells, within-cell application of ifenprodil (6 cells/5 rats) reversed the cocaine-induced increases in response amplitudes at both negative and positive holding potentials. 40 mV: cocaine WD > 39 versus cocaine WD > 39 + ifenprodil, paired t test, $t_{(5)} = 4.578$, $p = 0.006$; -80 mV: cocaine WD > 39 versus cocaine WD > 39 + ifenprodil, paired t test, $t_{(5)} = 3.46$, $p = 0.018$. **G,** Representative traces. Calibration: 40 mV, 50 pA \times 250 ms; -80 mV, 20 pA \times 250 ms. * $p < 0.05$.

Results

Enhanced NMDAR transmission precedes the delayed insertion of CP-AMPA after cocaine withdrawal

We first assessed whether pharmacologically isolated, electrically evoked NMDAR-mediated EPSCs onto MSNs in NAc core are altered after 39 d of withdrawal from cocaine self-administration (>WD39; Fig. 1A), when CP-AMPA transmission is stably elevated (Wolf and Tseng, 2012). To optimize between-group comparisons, stimulation intensities were adjusted to elicit a ~ 50 pA response at -20 mV, and changes in NMDAR EPSCs were compared at both negative and positive potentials without normalizing the responses to

40 mV or to the reversal potential. Relative to saline controls, recordings from cocaine WD > 39 rats showed a higher EPSC_{NMDA} peak amplitude at both negative (-80 mV) and positive (40 mV) holding potentials (Fig. 1B,C). Data obtained from earlier withdrawal times indicate that the enhanced NMDAR response in cocaine-treated rats begins to emerge as early as WD5 when the EPSC_{NMDA} peak amplitude recorded at 40 mV matches that of WD > 39 (Fig. 1D,E). By WD13, the EPSC_{NMDA} peak amplitudes recorded at both negative and positive potentials are indistinguishable from those observed after WD39 (Fig. 1D,E). Given that the amplitude of EPSC_{NMDA} recorded from WD1–WD3 and WD4 did not differ from saline controls, it is likely that the enhanced NMDAR transmission observed after WD39 results from withdrawal-dependent processes, rather than cocaine self-administration alone. Of note, the potentiation of NMDAR-EPSCs in the cocaine WD > 39 group is not associated with a change in EPSC_{NMDA} reversal potential, nor did reversal potentials differ significantly between cocaine rats recorded at the four withdrawal times shown in Figure 1D (saline: 9.8 ± 1.4 ; WD1–WD3: 9.9 ± 0.8 ; WD4: 11.9 ± 0.8 ; WD5: 10.5 ± 1.0 ; WD13–WD20: 10.6 ± 1.6 ; WD > 39: 10.5 ± 0.8 ; $p = 0.7$, one-way ANOVA).

Increased GluN2B contribution to the enhanced NMDAR transmission after cocaine withdrawal

We examined the relative contribution of GluN2B transmission to the enhanced EPSC_{NMDA} observed after WD39 by means of bath application of ifenprodil ($5 \mu\text{M}$, 10 min). Consistent with prior results in drug-naive rats (Chapman et al., 2003; Kasanetz and Manzoni, 2009), the effect of ifenprodil in MSNs from saline control rats was apparent only at the 40 mV holding potential as revealed by the amplitude of the evoked EPSC_{NMDA} (Fig. 2A,B,G). A similar effect was observed in MSNs recorded from cocaine rats, indicating that a GluN2B-mediated component could contribute to the enhanced EPSC_{NMDA} observed at 40 mV following cocaine withdrawal at WD5 (Fig. 2C,D,G) and WD > 39 (Fig. 2E–G). However, further analyses revealed that a similar proportion of the EPSC_{NMDA} at 40 mV was sensitive to ifenprodil in MSNs recorded from saline rats and from cocaine WD > 39 and cocaine WD5 rats ($47.1 \pm 9.1\%$ vs $47.3 \pm 5.7\%$, $45.1 \pm 4.6\%$, respectively). Remarkably, ifenprodil produced a significant reduction in EPSC_{NMDA} at -80 mV in cocaine WD > 39 rats (Fig. 2F), and a trend was seen in cocaine WD5 rats ($p = 0.12$) (Fig. 2D). The reduction at -80 mV was not apparent in MSNs from saline controls (Fig. 2B). Collectively, these results suggest that GluN2B transmission together with other ifenprodil-sensitive currents are driving the

enhanced EPSC_{NMDA} observed after prolonged withdrawal from cocaine self-administration.

Contribution of GluN3- and GluN2B-containing NMDARs after cocaine withdrawal

GluN3-mediated currents are less sensitive to Mg²⁺ block (Pachernegg et al., 2012; Perez-Otano et al., 2016) and therefore could potentially account for the increased EPSC_{NMDA} amplitude recorded at negative potentials during cocaine withdrawal. Thus, the effect of the GluN3 antagonist TK30 (30 μM) (Kvist et al., 2013) was used to determine the relative contribution of GluN3 transmission to the enhanced EPSC_{NMDA} observed in MSNs after WD39 from cocaine self-administration. Recordings obtained in the presence of TK30 revealed that the increased NMDAR transmission observed in MSNs from cocaine rats was attenuated, in particular at negative potentials (Fig. 3A). These results, along with the sequential changes in NMDAR currents observed during withdrawal (Fig. 1D,E) and the ifenprodil-sensitive EPSCs at both positive and negative potentials (Fig. 2E,F), suggest that at least two populations of GluN2B-containing NMDAR receptors with one also containing GluN3 are incorporated into synapses during cocaine withdrawal. To test this hypothesis, the effect of ifenprodil was examined in a subset of MSNs recorded in the presence of TK30 (Fig. 3B,C). We found that ifenprodil further reduced the attenuated EPSC_{NMDAR} amplitude elicited by TK30 at both positive (40 mV) and negative (−80 mV) potentials to saline control levels. Notably, bath application of TK30 did not affect EPSC_{NMDA} in saline controls (Fig. 3D), indicating that TK30 does not have off-target effects on the predominant NMDAR subtypes expressed in drug-naive MSNs, which include GluN2A and GluN2B subunits (Landwehrmeyer et al., 1995; Chapman et al., 2003; Dunah and Standaert, 2003; Logan et al., 2007; Kasanetz and Manzoni, 2009; Ma et al., 2009). Overall, these results support the hypothesis that the enhanced EPSC_{NMDAR} observed in NAc MSNs following prolonged withdrawal from cocaine self-administration is mediated by GluN2B and GluN3 transmission (Fig. 3E). We next performed the reverse experiment and found that no further changes of the reduced EPSC_{NMDAR} amplitude elicited by ifenprodil were observed after TK30 (Fig. 4A,B). Collectively, the data indicate that all GluN3-containing NMDARs also contain GluN2B, and that such receptors contribute to the enhanced NMDAR transmission observed at negative potentials after prolonged withdrawal from cocaine self-administration.

NMDAR-mediated Ca²⁺ entry into NAc spines after protracted cocaine withdrawal

Incorporation of either GluN3A or GluN3B into triheteromeric NMDARs substantially reduces Ca²⁺ permeability of the

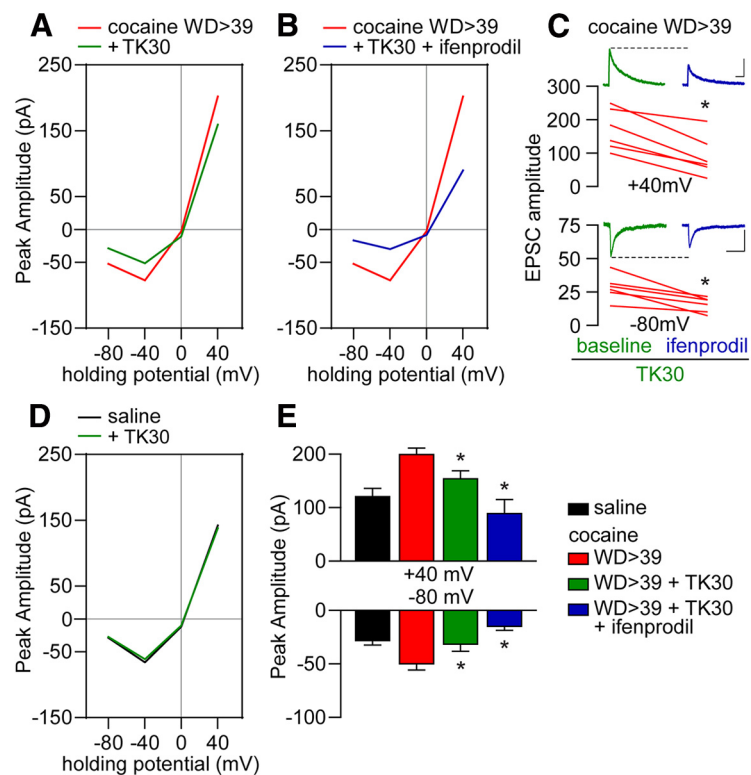


Figure 3. GluN3-containing NMDARs contribute to increased NMDAR function in cocaine WD > 39 cells but not under saline conditions. **A**, *I*–*V* plot of NMDAR-mediated synaptic responses of cocaine WD > 39 cells (from Fig. 1) compared with cocaine WD > 39 cells incubated with the GluN3 antagonist TK30 (30 μM; 13 cells/10 rats). **B**, *I*–*V* plot of NMDAR-mediated synaptic responses of a subgroup of TK30-incubated cocaine WD > 39 cells (6 cells/5 rats) that received subsequent bath application of ifenprodil (5 μM). **C**, For cells from **B**, comparison of TK30 baseline EPSCs to those recorded after ifenprodil application revealed further reductions in response amplitudes at both positive and negative holding potentials. 40 mV: cocaine WD > 39 + TK30 versus cocaine WD > 39 + TK30 + ifenprodil, paired *t* tests, *t*₍₅₎ = 6.01, *p* = 0.0018; −80 mV: cocaine WD39 + TK30 versus cocaine WD39 + TK30 + ifenprodil, paired *t* tests, *t*₍₅₎ = 4.24, *p* = 0.0082. Representative traces. Calibration: 40 mV, 50 pA × 250 ms; −80 mV, 20 pA × 250 ms. **D**, *I*–*V* plot showing the response amplitudes of saline cells before and after the application of TK30. **E**, Comparison of response amplitudes following bath application of TK30 and ifenprodil in cocaine WD > 39 cells. Saline data are for reference and were not included in analysis. ANOVA was used to analyze data for each holding potential, with comparisons conducted using Holm–Sidak *post hoc* tests: 40 mV: *F*_(2,45) = 10.18, *p* = 0.0002; cocaine WD > 39 versus +TK30 *p* = 0.044, cocaine WD > 39 versus +TK30 + ifenprodil *p* = 0.0003; +TK30 versus +TK30 + ifenprodil *p* = 0.044. −80 mV: *F*_(2,45) = 7.005, *p* = 0.0022; cocaine WD > 39 versus +TK30 *p* = 0.042; cocaine WD > 39 versus +TK30 + ifenprodil *p* = 0.005. **p* < 0.05.

receptor channel in expression systems (Pachernegg et al., 2012; Perez-Otano et al., 2016), and the same has been observed for GluN1/GluN2B/GluN3A triheteromeric receptors in the VTA of cocaine-exposed rats (Yuan et al., 2013). In contrast, increased Ca²⁺ permeability was reported for GluN3-containing triheteromeric receptors in somatosensory (Pilli and Kumar, 2012) and entorhinal (Beesley et al., 2019) cortices. To determine whether NMDAR-mediated Ca²⁺ entry is altered after protracted cocaine withdrawal when GluN3-NMDARs contribute to synaptic transmission, we imaged Ca²⁺ entry into dendritic spines of NAc core MSNs after photo-uncaging of MNI-NMDA (50 μM) in the presence of cadmium (100 μM) to block voltage-gated Ca²⁺ channels (Fig. 5). In saline controls, ~52% of dendritic spines responded to NMDA uncaging with Ca²⁺ entry, consistent with NMDAR expression in only a portion of striatal MSN spine synapses (Bernard and Bolam, 1998). Significantly fewer spines (~38%) responded in cocaine WD > 39 rats (Fig. 5A), while the magnitude of the Ca²⁺ transient in responding spines was not affected (Fig. 5B). Based on findings explained below (see Analysis of synaptic NMDAR subunit expression using PSD fractions and array tomography), this effect is not attributable to

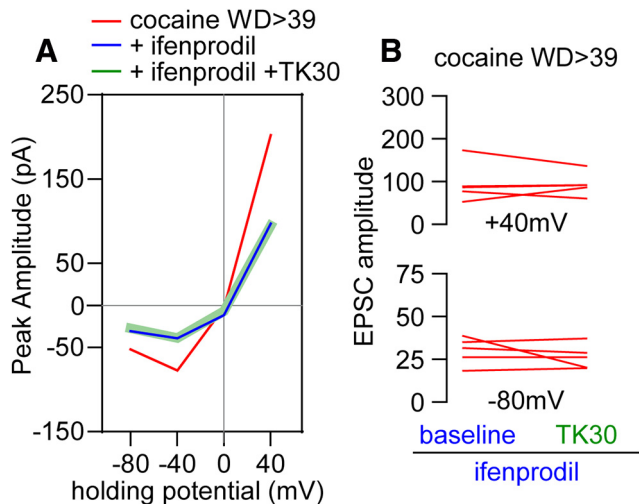


Figure 4. NMDAR subunit composition revealed by sequential application of GluN2B and GluN3 antagonists. **A**, *I*–*V* plot of cocaine WD > 39 data (for reference) and cocaine WD > 39 cells incubated with ifenprodil (5 μ M) followed by TK30 (30 μ M) application (5 cells/5 rats). **B**, TK30 application following ifenprodil produces no further decrease in response amplitude at 40 mV [cocaine WD > 39 + ifenprodil vs cocaine WD > 39 + ifenprodil + TK30, paired *t* test, $t_{(4)} = 0.20$, $p = 0.85$] or –80 mV [cocaine WD > 39 + ifenprodil vs cocaine WD > 39 + ifenprodil + TK30, paired *t* test, $t_{(4)} = 0.91$, $p = 0.41$]. These data suggest that all GluN3-containing NMDARs in cocaine WD > 39 cells also contain GluN2B (GluN1/GluN2B/GluN3 receptors), whereas data from Figure 3 suggest that these cells also express a population of NMDARs containing GluN2B but not GluN3.

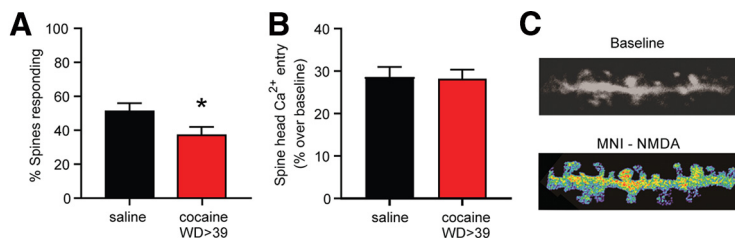


Figure 5. Fewer MSN dendritic spines respond to photo-uncaging of MNI-NMDA after prolonged withdrawal from cocaine self-administration. **A**, Percent of spines responding to MNI-NMDA (50 μ M) in cocaine rats ($n = 122$ spines; 10 cells; 4 rats) versus saline rats ($n = 135$ spines; 10 cells; 5 rats) [unpaired *t* test, $t_{(255)} = 2.290$, $p = 0.023$]. **B**, The magnitude of Ca^{2+} responses [($F_0/\Delta F - 1$) $\times 100$] in “responding” spines did not differ between treatment groups [unpaired *t* test, $t_{(114)} = 0.113$, $p = 0.91$]. **C**, Representative images showing Ca^{2+} influx in a dendritic segment from a cocaine animal in response to MNI-NMDA uncaging. * $p < 0.05$

altered spine density. These results are consistent with incorporation of NMDARs with lower Ca^{2+} permeability into a subset of NAc spines after cocaine withdrawal, and with our previous results using caged glutamate in the presence of CNQX (Ferrario et al., 2012).

Analysis of surface-expressed NMDAR subunits

To determine whether the observed NMDAR plasticity was detectable biochemically, we began by measuring cell surface and total NMDAR subunit levels using NAc tissue (primarily core) from saline and cocaine rats (WD2, WD14, WD25, and WD48) that had been prepared and biotinylated for use in prior studies (Loweth et al., 2014). These withdrawal times either precede any plasticity (WD2), coincide with the onset of GluN3 plasticity but precede any change in AMPAR subunit composition (WD14), target the period when CP-AMPA receptors begin to emerge (WD25), or target a period when both NMDAR and CP-AMPA receptor plasticity are well established (WD48). GluN1, GluN2A, GluN2B, and GluN3A were analyzed for all WDs. Gels for GluN3B

were run after the other subunits; by this time, the only samples remaining were surface fractions from WD48 saline and cocaine rats. No significant group differences were observed for cell surface GluN1, GluN2A, or GluN2B at any withdrawal time, and there was no difference in GluN3B surface expression on WD48 (Fig. 6). For GluN3A, there was a significant increase in surface expression in the cocaine group on WD48; on WD14 and WD25, the mean GluN3A surface expression in the cocaine group was similar to that of WD48 but did not achieve significance because of greater variability (Fig. 6). Considering these trends, this parallels the time course of GluN3A's contribution to synaptic transmission as determined with electrophysiology (Figs. 1 and 3). Total protein measured in starting material did not differ between saline and cocaine groups for any subunit at any of the withdrawal time points (data not shown). We note that a prior study reported alterations in GluN1 levels in NAc homogenates during incubation of cocaine craving, but these results are difficult to compare to ours because a core + shell homogenate was studied and because control rats self-administered sucrose (Lu et al., 2003).

Analysis of synaptic NMDAR subunit expression using PSD fractions and array tomography

To more selectively analyze the synaptic compartment, we measured NMDAR subunit protein levels in a Triton-insoluble PSD fraction prepared from the NAc (primarily core subregion) of different cohorts of saline and cocaine rats (WD5 and WD40) than those used for biotinylation studies. In light of biotinylation results, we were surprised that PSD fractions from saline and cocaine groups contained similar levels of GluN3A; GluN1, GluN2A, GluN2B, and GluN3B were also unchanged in the PSD fraction (Fig. 7).

To study NMDAR subunits with higher anatomic resolution, we used array tomography paired with serial antibody labeling of dendritic segments (Neuman et al., 2015). Individual NAc core MSNs in slices from saline rats (WD > 38) and cocaine rats (WD46–WD47) were labeled with biocytin, and tissue was then processed under experimenter-blind conditions to serially stain ultrathin sections with antibodies to GluA1, GluA2, GluN1, GluN2B, GluN3A, and GluN3B (Fig. 8A). Analysis revealed that saline and cocaine rats did not differ in total spine density in the NAc core (we did not quantify spine subtypes classified based on morphology) (Fig. 8B). We then performed spot analysis. A spot is a continuous collection of immunopositive pixels that colocalizes with the spine-head. Using this information, we conducted pairwise analysis of colocalization, defined as the percent of time that spots for two subunits are within 0.2 μ m. An increase in colocalization defined in this manner is interpreted as an increase in proximity of receptors containing each subunit, rather than an increase in tetramers containing both subunits. The cocaine group exhibited a trend ($p = 0.10$) toward reduced spots/spine for GluA2 (Fig. 8C), as well as significantly decreased colocalization of GluA1 and GluA2 (Fig. 8D). These results are consistent with a smaller relative contribution of GluA2-containing AMPARs to synaptic transmission after

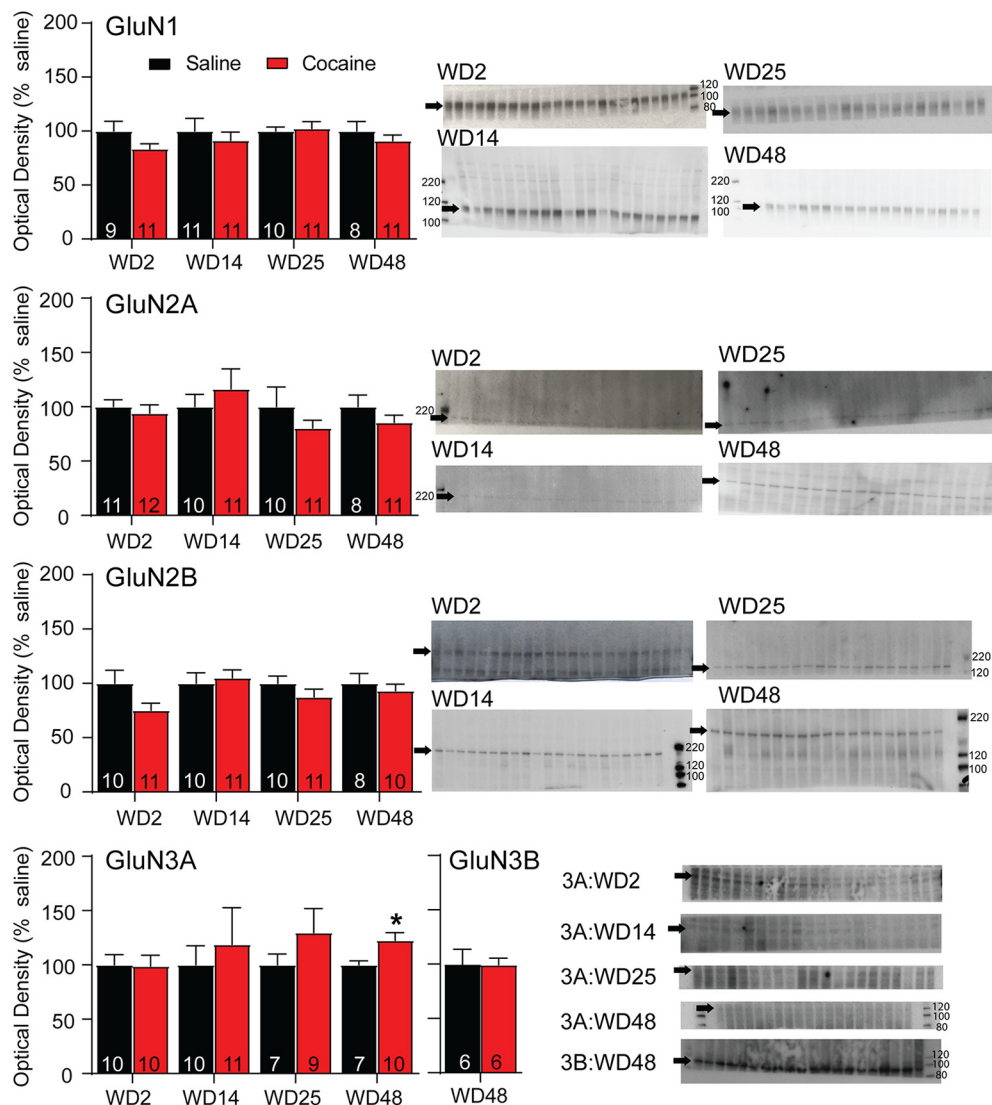


Figure 6. Cell surface expression of GluN3A, but not other NMDAR subunits, is altered after withdrawal from extended-access cocaine self-administration. NAc tissue from saline and cocaine rats killed on WD2, WD14, WD25, or WD48 was biotinylated to selectively label cell surface proteins and those biotinylated proteins were recovered and analyzed by immunoblotting as described in Materials and Methods. Dissected tissue was primarily from the core subregion. Left, Summary data (mean \pm SEM) comparing surface-expressed levels of each NMDAR subunit at different withdrawal times (data normalized to saline control groups). Right, Representative immunoblots are shown for each subunit at each withdrawal time. Arrows indicate band analyzed (GluN1 \sim 120 kDa, GluN2A \sim 180 kDa, GluN2B \sim 200 kDa, GluN3A \sim 125 kDa, GluN3B \sim 100 kDa). With the exception of a significant increase in surface GluN3A in the cocaine group on WD48 ($t_{(15)} = 2.44$, $p = 0.028$), NMDAR subunit protein levels did not differ between cocaine and saline groups at any withdrawal time. The number of tissue samples included in data analysis for each group is indicated within the bars. These values are sometimes smaller than the number of lanes shown because imperfections in the gel/blot interfered with analysis of a particular lane. Blots were cut to enable us to probe for a high molecular weight protein on one half and a low molecular weight protein on the other. Not all gels were cut at the same place; rather, they were cut to optimize the testing of more than one antibody based on the molecular weight of target proteins. * $p < 0.05$, Student's t test at each WD time point, saline versus cocaine.

incubation of cocaine craving (Conrad et al., 2008). Cocaine rats also demonstrated an increased average number of spots/spine for GluN3B (Fig. 8C) and increased colocalization in spines of GluN2B and GluN3B and of GluN3A and GluN3B (Fig. 8D).

Because spot analysis is not sensitive to changes in spot size, we also analyzed the total volume of immunoreactive puncta that colocalize with the spine for each subunit. These results are expressed as average puncta volume (Fig. 8E) as well as frequency histograms for each subunit (Fig. 8F–J). Based on the average of all antibodies (Fig. 8E, far-right bar) and histograms for GluA1, GluA2, GluN2B, and GluN3A (Fig. 8F–I), puncta volumes tended to be smaller after incubation, which might indicate that smaller, thin spines are more prevalent. The exception is GluN3B, which showed a rightward shift after incubation (Fig. 8H). Overall, these results and results presented above on overall

spine density (Fig. 8B) are generally consistent with our prior study of spines in the NAc core over 2 months of withdrawal from the same cocaine regimen; the only change detected was an increase in thin spines between WD25 and WD39, which reversed by WD60 (Christian et al., 2017). We note that spine density in the NAc shell is differently regulated during incubation of cocaine craving (Wright et al., 2020).

It is interesting that GluN3 data across different experiments parallels what we have found previously for GluA1 in the NAc core of “incubated” rats (Conrad et al., 2008; Ferrario et al., 2011b), namely, detection of a clear contribution to synaptic transmission in electrophysiological studies (for GluN3 subunits in general) and an increase in cell surface levels (GluN3A only) but no significant change in abundance in PSD fractions (GluN3A and GluN3B). For GluA1, these and other biochemical

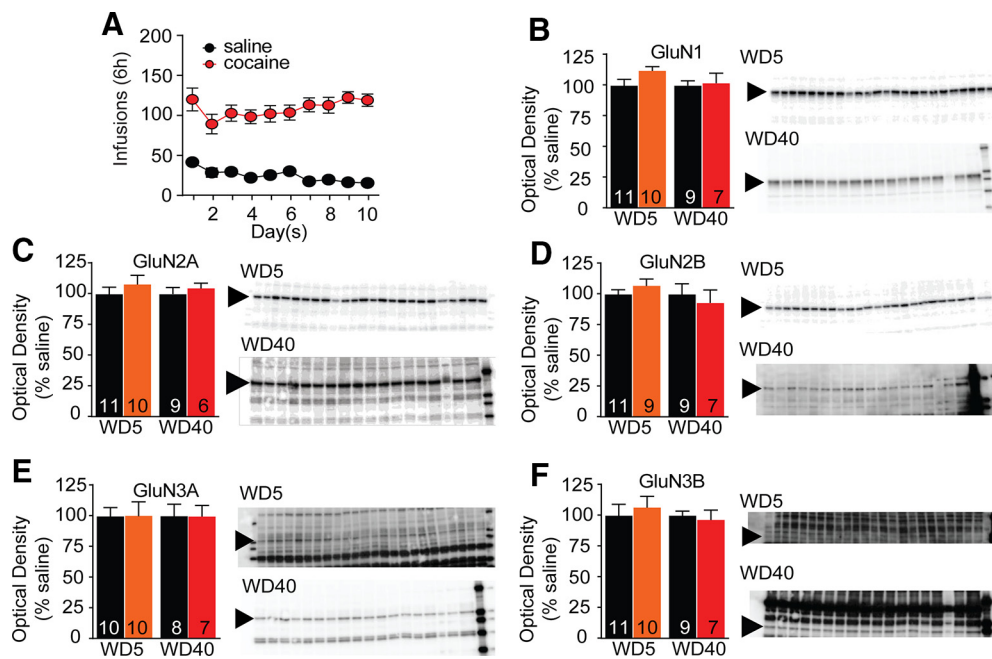


Figure 7. NMDAR subunit protein levels in PSD fractions are unaltered after withdrawal from extended-access cocaine self-administration. **A**, Self-administration training data for all animals included in this experiment. **B–F**, Triton-insoluble PSD fractions were prepared from the NAc of saline and cocaine rats killed on WD5 or WD40, as described in Materials and Methods. Dissected tissue was primarily from the core subregion. Summary data (mean \pm SEM) and representative immunoblots are shown for each subunit. Arrows indicate band analyzed (GluN1 \sim 120 kDa, GluN2A \sim 180 kDa, GluN2B \sim 200 kDa, GluN3A \sim 125 kDa, GluN3B \sim 100 kDa). NMDAR subunit protein levels did not differ between cocaine and saline groups at either withdrawal time. The number of tissue samples included in data analysis for each group is indicated within the bars. These values are sometimes smaller than the number of lanes shown either because imperfections in the gel/blot interfered with analysis of a particular lane or because behavioral data (analyzed after gels were run) revealed that rats did not reach criteria for discrimination of active versus inactive holes or stable self-administration during training. Blots were cut to enable us to probe for a high molecular weight protein on one half and a low molecular weight protein on the other. Not all gels were cut at the same place; rather, they were cut to optimize the testing of more than one antibody based on the molecular weight of target proteins. Student's *t* test at each WD time point, saline versus cocaine, NS.

results were interpreted to indicate that homomeric GluA1 CP-AMPA receptors contributing to synaptic transmission are loosely tethered to the PSD (possibly located at its margins) and are lost during preparation of PSD fractions (Ferrario et al., 2011b). A similar location for GluN3-NMDARs would not be surprising given the close interactions between homomeric GluA1 AMPARs and GluN3-NMDARs found in the VTA (Yuan et al., 2013). To explore this, we performed additional analyses of our array tomography data to estimate centrality versus laterality of glutamate receptor subunit expression in the PSD, taking advantage of the fact that all spines were stained for PSD95. First, we identified spine heads that exhibited puncta positive for both PSD95 and GluA1 (77 and 80 for saline and cocaine groups, respectively), PSD95 and GluN3A (52 and 41), or PSD95 and GluN3B (31 and 51). Using PSD95 staining as a marker for the PSD, we then determined the average percent of GluA1, GluN3A, or GluN3B puncta that spatially overlapped $>50\%$ (central expression) or $<50\%$ (lateral expression) with PSD95 puncta, and compared the balance of expression between central and lateral compartments (Fig. 9). In saline rats, GluA1 was mainly central, whereas GluN3A and GluN3B were evenly distributed; but after cocaine withdrawal, GluA1 and GluN3B were significantly more lateral than central, whereas GluN3A did not exhibit a significant difference in its distribution. Next, we compared the percent lateral expression for each subunit between saline and cocaine groups (Fig. 9). Compared with spines from saline rats, those from cocaine rats showed a significant increase in lateral GluA1 and lateral GluN3B, but no significant change for GluN3A. In summary, GluA1 and GluN3B are more often located laterally relative to PSD95 in cocaine animals compared with saline controls. The relative increase in lateral GluA1,

combined with increased cell surface and total GluA1 protein levels after incubation (Conrad et al., 2008; Ferrario et al., 2011b), supports the addition of homomeric GluA1 CP-AMPA receptors at the periphery of the synapse after incubation. The relative increase in lateral GluN3B, combined with no change in surface or total GluN3B levels, may suggest a shift of GluN3B from central to lateral regions of the synapse or a redistribution from extracellular pools to lateral synaptic regions. Finally, although not statistically significant, there was a small shift toward central GluN3A after incubation (saline: 51.7% central; cocaine: 59.7% central) that could be functionally significant.

Collectively, the array tomography experiments reveal NMDAR subunit alterations at the level of dendritic spines that were not detectable with Western analysis of PSD fractions. These alterations involve the same subunits (GluN2B and GluN3 subunits) implicated by electrophysiological results (Figs. 2–4), although the adaptations revealed by array tomography are more complex than might have been expected based on the electrophysiological results and clearly warrant further investigation.

GluN3A is required for incubation of cocaine craving

Next, we determined whether GluN3 NMDAR plasticity is required for incubation. We focused on GluN3A because this isoform was identified as mediating acute cocaine-induced increases in GluN3-NMDARs and CP-AMPA receptors in VTA dopamine neurons (Yuan et al., 2013) and because we observed increased GluN3A surface expression, but no change in GluN3B surface expression, after incubation of craving (Fig. 6). Viral vectors expressing the active construct used previously (Yuan et al., 2013) or a control sequence were injected into the NAc core \sim 5 weeks before cocaine self-administration. This timing was

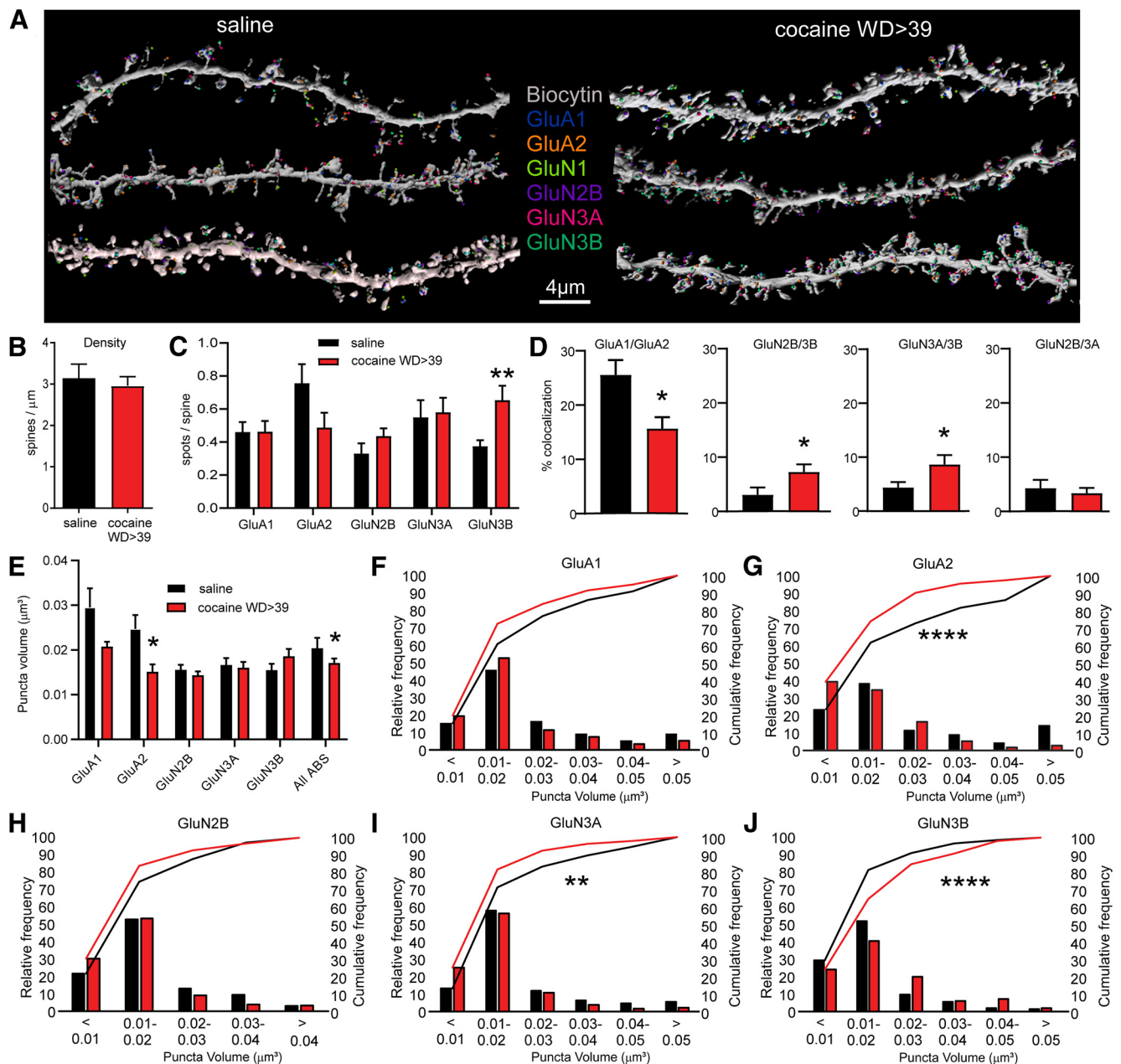


Figure 8. Array tomography analysis of AMPAR and NMDAR subunits in spines of NAc core MSN after saline or cocaine self-administration and protracted withdrawal. **A**, Representative labeling for each epitope in MSN dendrites after saline or cocaine self-administration. **B**, Spine density, determined from biocytin labeling, did not differ between groups (unpaired *t* test, $t_{19} = 0.43$). **C**, Average number of spots/spine was elevated for GluN3B (unpaired *t* test, $t_{19} = 3.20$, $p = 0.0047$) but not for other subunits ($p > 0.05$). A spot is defined as a continuous collection of immunopositive pixels that colocalizes with the spine. **D**, Colocalization of spots (defined as spots within 0.2 μm of each other) was altered for some NMDAR subunit pairs in the cocaine group (unpaired *t* tests, saline vs cocaine: GluA1/GluA2, $t_{19} = 2.686$, $p = 0.0146$; GluN2B/3B, $t_{19} = 2.137$, $p = 0.046$; GluN3A/3B, $t_{19} = 2.283$, $p = 0.0340$) but interestingly was not altered for GluN2B/3A ($t_{19} = 0.4658$, $p = 0.6467$). Other subunit pairs were analyzed but are not shown (all *p* values > 0.05). **E**, As spot analysis is not sensitive to changes in spot size, we also measured volume of immunoreactive puncta for each subunit. Shown here is the average puncta volume for each subunit. Far-right bar represents the average for all antibodies (All ABS), which provides an estimate of spine volume (unpaired *t* tests, saline vs cocaine: GluA2, $t_{19} = 2.496$, $p = 0.0219$; All ABS, $t_{103} = 2.002$, $p = 0.0479$; for all other subunits, $p > 0.05$). **F–J**, Frequency distribution plots of puncta volume for each subunit. χ^2 tests were used for statistical comparison of saline and cocaine relative frequency: GluA1, $\chi^2(5) = 6.22$, $p = 0.2859$; GluA2, $\chi^2(5) = 25.81$, $p = 0.000098$; GluN2B, $\chi^2(4) = 7.94$, $p = 0.0938$; GluN3A, $\chi^2(5) = 15.91$, $p = 0.0071$; GluN3B, $\chi^2(5) = 28.24$, $p = 0.000033$. * $p < 0.05$. ** $p < 0.01$. **** $p < 0.0001$. Saline group (>WD38): 3 rats, 4 cells, 12 dendrites, 825 spines. Cocaine group (WD46–WD47): 2 rats, 4 cells, 9 dendrites, 965 spines.

used to ensure robust expression in early withdrawal. We verified virus expression and target knockdown using drug-naïve rats (Fig. 10C,D). Cocaine self-administration was not altered by GluN3A constructs compared with control viruses (Fig. 10A) and was comparable with our typical results (e.g., Fig. 1A). After the completion of training, each rat received a cue-induced seeking test (30 min); responding in previously active hole delivers cue but no cocaine) on WD1 to establish baseline craving and

again on WD44 to assess incubation. Whereas rats receiving the control construct exhibited significantly increased responding on WD44 versus WD1, rats in the active shRNA group did not, indicating that GluN3A knockdown prevented incubation of craving during withdrawal (Fig. 10B). Then, using a different cohort of rats that underwent incubation of cocaine craving but did not receive virus infusion, we acutely blocked GluN3-NMDARs via intra-NAc infusion of TK30 (30 μM in 0.5 μl/

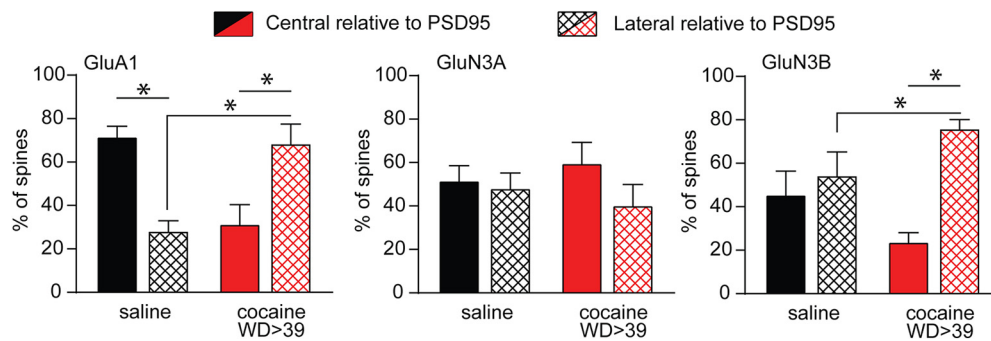


Figure 9. Glutamate receptor subunit localization relative to the PSD, defined by PSD95 staining, is altered after incubation of craving. Additional analysis of array tomography data was performed to estimate centrality versus laterality of glutamate receptor subunit expression in the PSD, focusing on spine heads exhibiting punctae positive for both PSD95 and GluA1 (77 and 80 for saline and cocaine groups, respectively), PSD95 and GluN3A (52 and 41), or PSD95 and GluN3B (31 and 51). Bar graphs represent the average percent of GluA1, GluN3A, or GluN3B punctae that spatially overlapped >50% (central expression) or <50% (lateral expression) with PSD95 punctae. First, for each subunit in each experimental group, the balance of expression between central and lateral compartments was compared using paired *t* tests: saline GluA1, $t_{(10)} = -3.97$, $p = 0.003$; saline GluN3A, $t_{(9)} = -0.217$, $p = 0.83$; saline GluN3B, $t_{(9)} = 0.383$, $p = 0.71$; cocaine GluA1, $t_{(9)} = -2.47$, $p = 0.04$; cocaine GluN3A, $t_{(9)} = -0.93$, $p = 0.38$; cocaine GluN3B, $t_{(9)} = 4.86$, $p = 0.002$ (* $p < 0.05$). We also compared the percent lateral expression for each subunit between saline and cocaine groups using one-way ANOVA: GluA1, $F_{(1,17)} = 18.3$, $p = 0.0005$; GluN3A, $F_{(1,16)} = 0.35$, $p = 0.56$; GluN3B, $F_{(1,15)} = 5.76$, $p = 0.03$ (* $p < 0.05$). Because these data are expressed as percent control, central locations are the inverse of lateral locations, so where there was a significant increase in laterality, there was also a significant reduction in centrality. For clarity, only significant changes in laterality are indicated by lines/asterisks in the figure.

hemisphere) just before a cue-induced seeking test in late withdrawal. There was no effect of TK30 on the expression of incubated cocaine seeking (Fig. 10E). Nose-pokes in the inactive hole and locomotor activity during the test were also unaffected (Fig. 10F,G). For all rats included in behavioral analysis, virus expression and location in the NAc core were confirmed as described in Experimental design and statistical analysis. Overall, these results suggest that GluN3 is a key component for incubation of craving but that, once incubation has occurred, GluN3 is not essential for its expression. In light of array tomography data indicating cocaine-induced plasticity involving GluN3B, future experiments should address the behavioral impact of its knockdown. It will also be important to determine whether GluN3A plasticity is required for the accumulation of CP-AMPA during the incubation of cocaine craving.

Although there was no difference in the relative contribution of GluN2B to NMDAR currents recorded at 40 mV in the saline and cocaine groups (Fig. 2) and no significant change in surface GluN2B after incubation (Fig. 6), our electrophysiological results suggest that GluN2B may assemble with GluN3 subunits (Figs. 3 and 4). Thus, we examined whether GluN2B in the NAc core was required for incubation of craving using a previously validated GluN2B RNAi (J. Wang et al., 2018). We verified virus expression and target knockdown using drug-naïve rats (Fig. 11C,D). Viral infusions, drug self-administration, and training were performed as described above (Fig. 11A), with cue-induced seeking tests conducted on WD1 and WD49 in both control and GluN2B RNAi rats (Fig. 11B). We found that GluN2B knockdown in NAc core before cocaine self-administration did not affect incubation (Fig. 11B), raising the interesting possibility of GluN3 assembly with other subunits under conditions of GluN2B depletion. For all rats included in behavioral analysis, virus expression and location in the NAc core were confirmed as described in Experimental design and statistical analysis.

Discussion

We showed previously that expression of “incubated” craving ultimately depends on CP-AMPA that accumulate in NAc core synapses after ~1 month of withdrawal (Conrad et al., 2008; Loweth et al., 2014; Wolf, 2016). Here, in the first study of NMDAR transmission in NAc core during incubation of cocaine

craving, we observed two waves of NMDAR plasticity, both preceding CP-AMPA elevation. An increase in currents mediated by GluN2B-containing NMDARs was first detected on WD5, and an increase mediated by GluN2B/GluN3-NMDARs was detected ~1 week later. Both populations then persisted through at least WD68. GluN3A knockdown prevented incubation, and it was the only subunit to show an increase in cell surface expression after incubation, consistent with prior work implicating GluN3A in addiction-related plasticity (Yuan et al., 2013; Creed et al., 2016; X. Huang et al., 2017). However, GluN2B and GluN3 subunit levels remained unchanged in PSD fractions, and more robust changes were observed for GluN3B than GluN3A at the single-spine level. These apparent inconsistencies could suggest that functional changes revealed by electrophysiology and Ca^{2+} imaging are associated with shifts in protein distribution too subtle to detect with biochemical analyses (e.g., redistribution from subsynaptic trafficking pools associated with the PSD to the synapse itself). It is also possible that these functional changes occur only at a subset of synapses onto MSN, and changes in protein levels in this subset may be washed out in biochemical studies by lack of changes in other synapses including synapses on other cell types. Finally, there are certainly gaps that remain in our understanding of synaptic plasticity associated with incubation of craving. Additional research may shed light on our observations. In particular, data from the dendritic spine level indicate that further study of GluN3B is warranted (see below). It will also be important for future research to determine whether mechanisms identified here hold for female rats.

Consequences of combined CP-AMPA and GluN3-NMDAR plasticity

In VTA dopamine neurons, acute cocaine injection rapidly increases both GluN2B/GluN3A-NMDARs and CP-AMPA, and the NMDAR plasticity is required for the AMPAR plasticity (Yuan et al., 2013). Thus, we hypothesize that GluN3-NMDARs are required for incubation because they promote the elevation of CP-AMPA on which incubation ultimately depends. We showed previously that a reduction in surface-expressed metabotropic glutamate receptor 1 (mGlu1) in NAc core during cocaine withdrawal is essential for subsequent CP-AMPA elevation (Loweth et al., 2014), consistent with evidence for an inverse

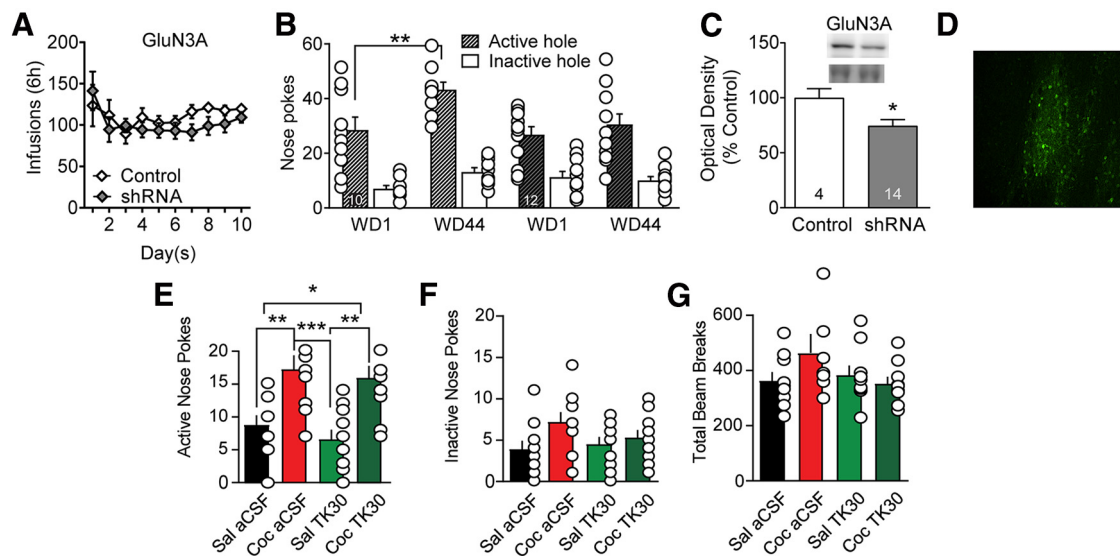


Figure 10. Viral knockdown of GluN3A in NAC core prevents incubation of cocaine craving but acute intra-NAC infusion of the GluN3 antagonist TK30 in late withdrawal does not prevent expression of incubated craving. **A**, GluN3A knockdown before cocaine self-administration did not impact drug taking during the training period. Mixed-effect analysis: self-administration day, $F_{(9,180)} = 2.329$, $p = 0.0167$; active versus control virus, $F_{(1,20)} = 0.8108$, NS; interaction (self-administration day vs active/control virus), $F_{(9,180)} = 0.8880$, NS. No significant *post hoc* tests (Holm–Sidak). **B**, GluN3A knockdown prevented incubation of craving, measured as increased cue-induced responding in the previously active nose-poke hole on WD44 versus WD1. With a three-way repeated-measures ANOVA (nose-poke hole \times virus condition \times WD), we observed a significant WD \times virus condition interaction ($F_{(1,40)} = 4.144$, $p = 0.048$). In rats receiving control virus, Bonferroni-corrected planned comparisons demonstrated a significant increase in nose-pokes from WD1 to WD44 ($p = 0.006$). Animals in the active shRNA virus group did not show incubation ($p = 0.323$). The same conclusion, namely, that the active shRNA virus blocked incubation, was supported if we conducted separate two-way repeated-measures ANOVAs for active and inactive hole responses (active hole: significant main effects for WD [$F_{(1,39)} = 5.564$, $p = 0.0234$] and virus condition [$F_{(1,39)} = 5.751$, $p = 0.0214$]; inactive hole: no significant main effects). **C**, Viral efficacy indicated by decreased GluN3A protein expression in NAC core of drug-naïve rats. Upper bands represent GluN3A, and lower bands represent a prominent Ponceau S-stained band from the same lane; Ponceau staining in the entire lane was our measure of protein loading. Unpaired *t* test: control versus GluN3A shRNA ($t_{(16)} = 2.169$, $p < 0.05$). **D**, Visualization of virus expression based on GFP fluorescence in NAC core of a representative drug-naïve rat. Scale bar, 50 μm . **E–G**, Microinjection of TK30 directly into the NAC core after protracted withdrawal from extended-access cocaine self-administration does not prevent expression of incubated cocaine seeking. Rats self-administered saline or cocaine as in previous experiments. Each rat underwent two cue-induced seeking tests (WD35 and WD42). One hour before the first seeking test, aCSF (control) or TK30 (GluN3-selective antagonist; 30 μM in 0.5 μl /hemisphere) was injected bilaterally into the NAC core of 10 rats (5 received aCSF and 5 received TK30). Seven days later (WD42), using a crossover design, aCSF or TK30 was injected bilaterally into the NAC core of the same rats 1 h before the second seeking test. This yielded four experimental groups: Sal aCSF, Coc aCSF, Sal TK30, and Coc TK30 ($n = 10$ observations per group). Compared with aCSF injection, TK30 injection had no effect on active hole responding (**E**), inactive hole responding (**F**), or locomotor activity during the test (**G**) in either saline or cocaine rats; that is, cocaine rats expressed incubation regardless of whether they were pretreated with aCSF or TK30. Thus, activation of GluN3-containing NMDARs during a seeking test is not required for the expression of incubation, although their synaptic incorporation during cocaine withdrawal is necessary for incubation to occur (**B**). We note that active hole responding in the cocaine late withdrawal groups in **E** is lower than for cocaine late withdrawal groups in **B**. This is likely because the former groups received an intracranial injection immediately before the test, which typically lowers active hole responding. **E–G**, Data were analyzed using one-way ANOVA with Holm–Sidak *post hoc* tests. **E**, Active hole: $F_{(3,36)} = 8.744$, $p = 0.0002$; saline aCSF versus cocaine aCSF, $p = 0.0093$; saline aCSF versus cocaine TK30, $p = 0.0342$; cocaine aCSF versus saline TK30, $p = 0.0008$; saline TK30 versus cocaine TK30, $p = 0.0035$. **F**, Inactive hole: $F_{(3,36)} = 2.034$, $p = 0.1265$. **G**, Locomotor activity: $F_{(3,36)} = 2.034$; $p = 0.1265$. * $p < 0.05$. ** $p < 0.01$. *** $p < 0.001$.

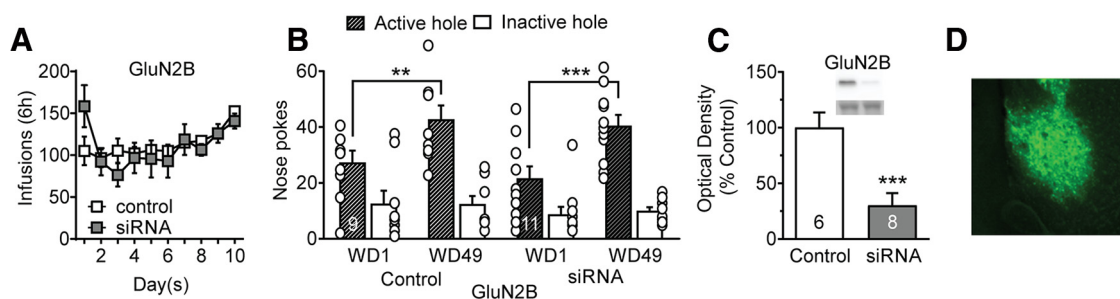


Figure 11. Viral knockdown of GluN2B in NAC core does not influence incubation of cocaine craving during withdrawal. **A**, GluN2B knockdown before cocaine self-administration did not impact drug taking during the training period. Mixed-effect analysis: self-administration day, $F_{(9,155)} = 4.476$, $p < 0.0001$; active versus control virus, $F_{(1,18)} = 0.02696$, NS; interaction (self-administration day vs active/control virus), $F_{(9,155)} = 1.568$, NS. *Post hoc* tests were not significant (Holm–Sidak). **B**, GluN2B knockdown did not prevent incubation of craving, measured as increased cue-induced responding in the previously active nose-poke hole on WD49 versus WD1. A three-way repeated-measures ANOVA (nose-poke hole \times virus condition \times WD) revealed a main effect of WD ($F_{(1,36)} = 9.477$, $p = 0.004$) but no significant WD \times virus condition interaction ($F_{(1,36)} = 0.1709$, NS). In both control and active siRNA groups, there was a significant increase in nose-pokes from WD1 to WD49 (Bonferroni-corrected planned comparisons: control WD1 vs WD49, $p = 0.0168$; siRNA WD1 vs WD49, $p = 0.0003$). **C**, Viral efficacy indicated by decreased GluN2B protein expression in NAC core of drug-naïve rats. Upper bands represent GluN2B, and lower bands represent a prominent Ponceau S-stained band from the same lane; Ponceau staining in the entire lane was our measure of protein loading. Unpaired *t* test: control versus GluN2B siRNA ($t_{(12)} = 4.02$, $p < 0.001$). **D**, Visualization of virus expression based on GFP fluorescence in NAC core of a representative drug-naïve rat. Scale bar, 50 μm . ** $p < 0.01$, *** $p < 0.001$.

relationship between CP-AMPA receptors and mGlu1 tone in many brain regions (Loweth et al., 2013). Given that mGlu1 negatively regulates GluN3 incorporation in the VTA (Yuan et al., 2013), it is possible that the reduction in NAc mGlu1, which occurs at about the same withdrawal time as elevation of GluN3-NMDARs (see Loweth et al., 2014), triggers GluN3-NMDAR plasticity, which in turn enables CP-AMPA receptor plasticity.

What is driving this cascade of plasticity? Multiple lines of evidence suggest a relative decrease in excitatory drive to MSNs and/or their excitability during early withdrawal from cocaine self-administration (Wolf, 2016). Synaptic incorporation of GluN3-NMDARs, which increase NMDAR currents at negative potentials because of insensitivity to Mg^{2+} block (Pachernegg et al., 2012; Perez-Otano et al., 2016), and CP-AMPA receptors, which have higher single-channel conductance than GluA2-containing AMPARs (Isaac et al., 2007), may represent a homeostatic response designed to maximize the MSNs' ability to respond under such conditions, albeit with the maladaptive consequence of boosting the response to strong excitatory signals elicited by drug cues. Consistent with this homeostatic hypothesis, in hippocampus, synaptic activity leads to GluN3-NMDAR endocytosis, whereas inactivity promotes their accumulation (Perez-Otano et al., 2006).

Along with reduced sensitivity to Mg^{2+} block, GluN3-NMDARs display reduced Ca^{2+} permeability (Pachernegg et al., 2012; Perez-Otano et al., 2016). Consistent with this, we found that fewer MSN spines from "incubated" rats exhibited Ca^{2+} entry in response to NMDA uncaging. In VTA dopamine neurons after acute cocaine injection, a shift from NMDAR-mediated to CP-AMPA-mediated Ca^{2+} entry accompanied insertion of GluN3-NMDARs and CP-AMPA receptors, leading to a shift from Hebbian to anti-Hebbian LTP (Mameli et al., 2011). We speculate that coexistence of GluN3-NMDARs and CP-AMPA receptors in the NAc core after incubation of cocaine craving similarly alters the rules for synaptic plasticity and, by extension, affects subsequent reward learning. Furthermore, it is interesting that CP-AMPA receptors and GluN3-NMDARs are typically associated with immature synapses, and their coexpression in postnatal VTA is proposed to sculpt developmental plasticity (Yuan and Bellone, 2013). Thus, our findings, along with the recent demonstration that prenatal nicotine exposure may upregulate GluN3-NMDARs along with CP-AMPA receptors (Polli and Kohlmeier, 2018, 2019), resonate with theories that drugs of abuse reopen mechanisms that permit dramatic plasticity during development (Bellone and Luscher, 2012; Dong and Nestler, 2014). A relative increase in Ca^{2+} entry via AMPARs versus NMDARs may also affect many Ca^{2+} -sensitive signaling pathways. For example, Ca^{2+} entry through NMDARs suppresses protein translation (Scheetz et al., 2000; Reese and Kavalali, 2015), so incorporation of Ca^{2+} -impermeable GluN3-NMDARs may explain why NMDAR-mediated suppression of translation is lost in NAc tissue from "incubated" rats (Stefanik et al., 2018).

Regulation of synaptic GluN3-NMDAR levels

Slice recordings demonstrated that a contribution of GluN3-NMDARs to synaptic transmission emerges after ~2 weeks of cocaine withdrawal and is then maintained (>WD39). This is paralleled by trends toward increased cell surface GluN3A on WD14 and WD25 in cocaine versus saline groups and a significant increase on WD48. Surface GluN2B did not change at any withdrawal time, and surface GluN3B was unaltered on WD48. These results are consistent with the ability of GluN3A but not GluN2B knockdown to prevent incubation of craving.

In contrast to biotinylation results, saline and cocaine groups did not differ in GluN3A abundance in a Triton-insoluble PSD

fraction on WD5 or WD40; GluN3B was also unaltered. Likewise, their abundance was unaltered in NAc membrane fractions after 2 weeks withdrawal from binge-access cocaine self-administration (Tang et al., 2004). As noted in Results, this profile for GluN3A (detection of increased contribution to synaptic transmission in electrophysiological studies and an increase in cell surface levels, but no significant change in abundance in PSD fractions) parallels previous findings for GluA1 (Conrad et al., 2008; Ferrario et al., 2011b), which we interpreted to indicate that homomeric GluA1 receptors contributing to synaptic transmission are located at the margins of synapses and thus loosely tethered to the PSD (Ferrario et al., 2011b). The present array tomography results support this interpretation, as GluA1 becomes more enriched in lateral portions of the synapse after incubation of craving. While this was also observed for GluN3B, it was not observed for GluN3A, which was evenly distributed in both saline and cocaine rats. As noted above (first paragraph of Discussion), there may be shifts in NMDAR subunit levels or distribution that are functionally significant but too subtle to detect with biochemical methods, particularly if such changes are limited to a subpopulation of synapses. In hippocampus, both anatomic and biochemical evidence supports localization of GluN3A to lateral margins of synapses (Perez-Otano et al., 2006; Wee et al., 2016).

While our electrophysiological studies isolated NMDAR-mediated currents, GluN1/GluN3 glycine receptors could contribute to biochemical and array tomography findings and thereby complicate their interpretation. Future studies could address the functional role of GluN1/GluN3 glycine receptors using approaches developed previously (Grand et al., 2018).

Comparison of core and shell plasticity during incubation

Incubation of cocaine craving requires both NAc core and shell subregions (Wolf, 2016; Dong et al., 2017; J. Wang et al., 2018). As in core, CP-AMPA receptors accumulate in shell synapses, and their activation is necessary for expression of incubation (Lee et al., 2013; Ma et al., 2014). The requirement for CP-AMPA receptor activation in both subregions may reflect their anatomic interconnections (Haber et al., 2000). In shell, CP-AMPA receptor accumulation results from a cascade of bidirectional homeostatic plasticity between the strength of excitatory synaptic input and the membrane excitability of MSNs. This cascade is initiated by an increase in synaptic GluN2B-NMDARs corresponding to silent synapses that begins during cocaine exposure and is robust by WD1 (Y. H. Huang et al., 2009); these silent synapses are subsequently filled by CP-AMPA receptors (Lee et al., 2013; Ma et al., 2014; Dong et al., 2017; J. Wang et al., 2018). As would be predicted, knocking down GluN2B in NAc shell prevents this cascade and thereby prevents incubation (J. Wang et al., 2018). A different cascade appears to account for CP-AMPA receptor accumulation in NAc core (although this cascade may also involve homeostatic plasticity, as described above in Consequences of combined CP-AMPA receptor and GluN3-NMDAR plasticity). In the core, increased GluN2B-NMDARs are first detected on WD5, and GluN2B knockdown does not prevent incubation. The latter is surprising because incubation was prevented by GluN3A knockdown in NAc core and our electrophysiological results indicate that the GluN3-NMDARs observed after cocaine withdrawal also contain GluN2B. It is possible that GluN3 assembles with other subunits when GluN2B is depleted. Alternatively, our knockdown may have insufficiently depleted the GluN2B pool that assembles with GluN3.

That different plasticity occurs in core and shell subregions is not surprising, given their different connectivity and behavioral roles (Sesack and Grace, 2010). Future work should test whether

mechanisms identified in core (reduced mGlu1 and increased GluN3 contribution) apply in shell, and whether mechanisms identified in shell (silent synapse generation and synapse-to-membrane homeostatic plasticity) apply in core. It will also be important to determine cell type and input specificity of the observed NMDAR plasticity in NAc core, and investigate additional NMDAR subunits implicated in cocaine's actions (e.g., Joffe and Grueter, 2016).

In conclusion, a complex cascade of NMDAR and AMPAR plasticity in the NAc core leads to persistent increases in reactivity to cocaine cues and relapse vulnerability. This is a remarkable example of experience-dependent glutamatergic plasticity evolving over a protracted time frame in the adult nervous system.

References

- Beesley S, Sullenberger T, Pilli J, Abbasi S, Gunjan A, Kumar SS (2019) Colocalization of distinct NMDA receptor subtypes at excitatory synapses in the entorhinal cortex. *J Neurophysiol* 121:238–254.
- Bellone C, Luscher C (2012) Drug-evoked plasticity: do addictive drugs reopen a critical period of postnatal synaptic development? *Front Mol Neurosci* 5:75.
- Bernard V, Bolam JP (1998) Subcellular and subsynaptic distribution of the NR1 subunit of the NMDA receptor in the neostriatum and globus pallidus of the rat: co-localization at synapses with the GluR2/3 subunit of the AMPA receptor. *Eur J Neurosci* 10:3721–3736.
- Briggs CA, Schneider C, Richardson JC, Stutzmann GE (2013) beta amyloid peptide plaques fail to alter evoked neuronal calcium signals in APP/PS1 Alzheimer's disease mice. *Neurobiol Aging* 34:1632–1643.
- Chapman DE, Keefe KA, Wilcox KS (2003) Evidence for functionally distinct synaptic NMDA receptors in ventromedial versus dorsolateral striatum. *J Neurophysiol* 89:69–80.
- Chen J, Ma Y, Fan R, Yang Z, Li MD (2018) Implication of genes for the N-methyl-D-aspartate (NMDA) receptor in substance addictions. *Mol Neurobiol* 55:7567–7578.
- Christian DT, Wang X, Chen EL, Sehgal LK, Ghassemilou MN, Miao JJ, Estepanian D, Araghi CH, Stutzmann GE, Wolf ME (2017) Dynamic alterations of rat nucleus accumbens dendritic spines over 2 months of abstinence from extended-access cocaine self-administration. *Neuropsychopharmacology* 42:748–756.
- Conrad KL, Tseng KY, Uejima JL, Reimers JM, Heng LJ, Shaham Y, Marinelli M, Wolf ME (2008) Formation of accumbens GluR2-lacking AMPA receptors mediates incubation of cocaine craving. *Nature* 454:118–121.
- Creed M, Kauffling J, Fois GR, Jalabert M, Yuan T, Luscher C, Georges F, Bellone C (2016) Cocaine exposure enhances the activity of ventral tegmental area dopamine neurons via calcium-impermeable NMDARs. *J Neurosci* 36:10759–10768.
- Curras MC, Dao J (1998) Developmental plasticity of NR1 and NR2B subunit expression in the supraoptic nucleus of the rat hypothalamus. *Brain Res Dev Brain Res* 109:1–12.
- Davies KD, Alvestad RM, Coultrap SJ, Browning MD (2007) alphaCaMKII autophosphorylation levels differ depending on subcellular localization. *Brain Res* 1158:39–49.
- Davies KD, Goebel-Goody SM, Coultrap SJ, Browning MD (2008) Long term synaptic depression that is associated with GluR1 dephosphorylation but not alpha-amino-3-hydroxy-5-methyl-4-isoxazolepropionic acid (AMPA) receptor internalization. *J Biol Chem* 283:33138–33146.
- Dong Y, Nestler EJ (2014) The neural rejuvenation hypothesis of cocaine addiction. *Trends Pharmacol Sci* 35:374–383.
- Dong Y, Taylor JR, Wolf ME, Shaham Y (2017) Circuit and synaptic plasticity mechanisms of drug relapse. *J Neurosci* 37:10867–10876.
- Dunah AW, Standaert DG (2003) Subcellular segregation of distinct heteromeric NMDA glutamate receptors in the striatum. *J Neurochem* 85:935–943.
- Ferrario CR, Li X, Wang X, Reimers JM, Uejima JL, Wolf ME (2010) The role of glutamate receptor redistribution in locomotor sensitization to cocaine. *Neuropsychopharmacology* 35:818–833.
- Ferrario CR, Goussakov I, Stutzmann GE, Wolf ME (2012) Withdrawal from cocaine self-administration alters NMDA receptor-mediated Ca²⁺ entry in nucleus accumbens dendritic spines. *PLoS One* 7:e40898.
- Ferrario CR, Loweth JA, Milovanovic M, Wang X, Wolf ME (2011a) Distribution of AMPA receptor subunits and TARPs in synaptic and extrasynaptic membranes of the adult rat nucleus accumbens. *Neurosci Lett* 490:180–184.
- Ferrario CR, Loweth JA, Milovanovic M, Ford KA, Galinanes GL, Heng LJ, Tseng KY, Wolf ME (2011b) Alterations in AMPA receptor subunits and TARPs in the rat nucleus accumbens related to the formation of Ca²⁺-permeable AMPA receptors during the incubation of cocaine craving. *Neuropharmacology* 61:1141–1151.
- Garraway SM, Xu Q, Inturrisi CE (2009) siRNA-mediated knockdown of the NR1 subunit gene of the NMDA receptor attenuates formalin-induced pain behaviors in adult rats. *J Pain* 10:380–390.
- Goebel-Goody SM, Davies KD, Alvestad Linger RM, Freund RK, Browning MD (2009) Phospho-regulation of synaptic and extrasynaptic N-methyl-D-aspartate receptors in adult hippocampal slices. *Neuroscience* 158:1446–1459.
- Grand T, Abi Gerges S, David M, Diana MA, Paoletti P (2018) Unmasking GluN1/GluN3A excitatory glycine NMDA receptors. *Nat Commun* 9:4769.
- Grimm JW, Hope BT, Wise RA, Shaham Y (2001) Neuroadaptation: incubation of cocaine craving after withdrawal. *Nature* 412:141–142.
- Guillem K, Ahmed SH, Peoples LL (2014) Escalation of cocaine intake and incubation of cocaine seeking are correlated with dissociable neuronal processes in different accumbens subregions. *Biol Psychiatry* 76:31–39.
- Haber SN, Fudge JL, McFarland NR (2000) Striatonigrostriatal pathways in primates form an ascending spiral from the shell to the dorsolateral striatum. *J Neurosci* 20:2369–2382.
- Hansen KB, Yi F, Perszyk RE, Furukawa H, Wollmuth LP, Gibb AJ, Traynelis SF (2018) Structure, function, and allosteric modulation of NMDA receptors. *J Gen Physiol* 150:1081–1105.
- Hollander JA, Carelli RM (2005) Abstinence from cocaine self-administration heightens neural encoding of goal-directed behaviors in the accumbens. *Neuropsychopharmacology* 30:1464–1474.
- Hollander JA, Carelli RM (2007) Cocaine-associated stimuli increase cocaine seeking and activate accumbens core neurons after abstinence. *J Neurosci* 27:3535–3539.
- Huang X, Chen YY, Shen Y, Cao X, Li A, Liu Q, Li Z, Zhang LB, Dai W, Tan T, Arias-Carrion O, Xue YX, Su H, Yuan TF (2017) Methamphetamine abuse impairs motor cortical plasticity and function. *Mol Psychiatry* 22:1274–1281.
- Huang YH, Lin Y, Mu P, Lee BR, Brown TE, Wayman G, Marie H, Liu W, Yan Z, Sorg BA, Schluter OM, Zukin RS, Dong Y (2009) In vivo cocaine experience generates silent synapses. *Neuron* 63:40–47.
- Isaac JT, Ashby MC, McBain CJ (2007) The role of the GluR2 subunit in AMPA receptor function and synaptic plasticity. *Neuron* 54:859–871.
- Joffe ME, Grueter BA (2016) Cocaine experience enhances thalamo-accumbens N-methyl-D-aspartate receptor function. *Biol Psychiatry* 80:671–681.
- Kasanetz F, Manzoni OJ (2009) Maturation of excitatory synaptic transmission of the rat nucleus accumbens from juvenile to adult. *J Neurophysiol* 101:2516–2527.
- Khan AM, Curras MC, Dao J, Jamal FA, Turkowski CA, Goel RK, Gillard ER, Wolfsohn SD, Stanley BG (1999) Lateral hypothalamic NMDA receptor subunits NR2A and/or NR2B mediate eating: immunochemical/behavioral evidence. *Am J Physiol* 276:R880–R891.
- Kvist T, Greenwood JR, Hansen KB, Traynelis SF, Brauner-Osborne H (2013) Structure-based discovery of antagonists for GluN3-containing N-methyl-D-aspartate receptors. *Neuropharmacology* 75:324–336.
- Landwehrmeyer GB, Standaert DG, Testa CM, Penney JB Jr, Young AB (1995) NMDA receptor subunit mRNA expression by projection neurons and interneurons in rat striatum. *J Neurosci* 15:5297–5307.
- Lee BR, Ma YY, Huang YH, Wang X, Otaka M, Ishikawa M, Neumann PA, Graziane NM, Brown TE, Suska A, Guo C, Lobo MK, Sesack SR, Wolf ME, Nestler EJ, Shaham Y, Schluter OM, Dong Y (2013) Maturation of silent synapses in amygdala-accumbens projection contributes to incubation of cocaine craving. *Nat Neurosci* 16:1644–1651.
- Li X, Venniro M, Shaham Y (2016) Translational research on incubation of cocaine craving. *JAMA Psychiatry* 73:1115–1116.
- Logan SM, Partridge JG, Matta JA, Buonanno A, Vicini S (2007) Long-lasting NMDA receptor-mediated EPSCs in mouse striatal medium spiny neurons. *J Neurophysiol* 98:2693–2704.
- Loweth JA, Tseng KY, Wolf ME (2013) Using metabotropic glutamate receptors to modulate cocaine's synaptic and behavioral effects: mGluR1 finds a niche. *Curr Opin Neurobiol* 23:500–506.

- Loweth JA, Scheyer AF, Milovanovic M, LaCrosse AL, Flores-Barrera E, Werner CT, Li X, Ford KA, Le T, Olive MF, Szumlinski KK, Tseng KY, Wolf ME (2014) Synaptic depression via mGluR1 positive allosteric modulation suppresses cue-induced cocaine craving. *Nat Neurosci* 17:73–80.
- Lu L, Grimm JW, Shaham Y, Hope BT (2003) Molecular neuroadaptations in the accumbens and ventral tegmental area during the first 90 days of forced abstinence from cocaine self-administration in rats. *J Neurochem* 85:1604–1613.
- Ma YY, Cepeda C, Cui CL (2009) The role of striatal NMDA receptors in drug addiction. *Int Rev Neurobiol* 89:131–146.
- Ma YY, Lee BR, Wang X, Guo C, Liu L, Cui R, Lan Y, Balcita-Pedicino JJ, Wolf ME, Sesack SR, Shaham Y, Schluter OM, Huang YH, Dong Y (2014) Bidirectional modulation of incubation of cocaine craving by silent synapse-based remodeling of prefrontal cortex to accumbens projections. *Neuron* 83:1453–1467.
- Mameli M, Bellone C, Brown MT, Luscher C (2011) Cocaine inverts rules for synaptic plasticity of glutamate transmission in the ventral tegmental area. *Nat Neurosci* 14:414–416.
- McCutcheon JE, Loweth JA, Ford KA, Marinelli M, Wolf ME, Tseng KY (2011) Group I mGluR activation reverses cocaine-induced accumulation of calcium-permeable AMPA receptors in nucleus accumbens synapses via a protein kinase C-dependent mechanism. *J Neurosci* 31:14536–14541.
- Murray CH, Loweth JA, Milovanovic M, Stefanik MT, Caccamise AJ, Dolubizno H, Funke JR, Foster Olive M, Wolf ME (2019) AMPA receptor and metabotropic glutamate receptor 1 adaptations in the nucleus accumbens core during incubation of methamphetamine craving. *Neuropsychopharmacology* 44:1534–1541.
- Murray CH, Christian DT, Milovanovic M, Loweth JA, Hwang EK, Caccamise AJ, Funke JR, Wolf ME (2021) mGlu5 function in the nucleus accumbens core during the incubation of methamphetamine craving. *Neuropharmacology* 186:108452.
- Neuman KM, Molina-Campos E, Musial TF, Price AL, Oh KJ, Wolke ML, Buss EW, Scheff SW, Mufson EJ, Nicholson DA (2015) Evidence for Alzheimer's disease-linked synapse loss and compensation in mouse and human hippocampal CA1 pyramidal neurons. *Brain Struct Funct* 220:3143–3165.
- Pachernegg S, Strutz-Seeböhm N, Hollmann M (2012) GluN3 subunit-containing NMDA receptors: not just one-trick ponies. *Trends Neurosci* 35:240–249.
- Palma-Cerda F, Auger C, Crawford DJ, Hodgson AC, Reynolds SJ, Cowell JK, Swift KA, Cais O, Vyklicky L, Corrie JE, Ogden D (2012) New caged neurotransmitter analogs selective for glutamate receptor sub-types based on methoxynitroindoline and nitrophenylethoxycarbonyl caging groups. *Neuropharmacology* 63:624–634.
- Perez-Otano I, Lujan R, Tavalin SJ, Plomann M, Modregger J, Liu XB, Jones EG, Heinemann SF, Lo DC, Ehlers MD (2006) Endocytosis and synaptic removal of NR3A-containing NMDA receptors by PACSIN1/syndapin1. *Nat Neurosci* 9:611–621.
- Perez-Otano I, Larsen RS, Wesseling JF (2016) Emerging roles of GluN3-containing NMDA receptors in the CNS. *Nat Rev Neurosci* 17:623–635.
- Pickens CL, Airavaara M, Theberge F, Fanous S, Hope BT, Shaham Y (2011) Neurobiology of the incubation of drug craving. *Trends Neurosci* 34:411–420.
- Pietrogrande G, Zaleska K, Zhao Z, Abdolhosseini M, Chow WZ, Sanchez-Bezanilla S, Ong LK, Johnson SJ, Nilsson M, Walker FR (2019) Low oxygen post conditioning prevents thalamic secondary neuronal loss caused by excitotoxicity after cortical stroke. *Sci Rep* 9:4841.
- Pilli J, Kumar SS (2012) Triheteromeric N-methyl-D-aspartate receptors differentiate synaptic inputs onto pyramidal neurons in somatosensory cortex: involvement of the GluN3A subunit. *Neuroscience* 222:75–88.
- Plaza-Zabala A, Li X, Milovanovic M, Loweth JA, Maldonado R, Berrendero F, Wolf ME (2013) An investigation of interactions between hypocretin/orexin signaling and glutamate receptor surface expression in the rat nucleus accumbens under basal conditions and after cocaine exposure. *Neurosci Lett* 557B:101–106.
- Polli FS, Kohlmeier KA (2018) Prenatal nicotine exposure alters postsynaptic AMPA receptors and glutamate neurotransmission within the laterodorsal tegmentum (LDT) of juvenile mice. *Neuropharmacology* 137:71–85.
- Polli FS, Kohlmeier KA (2019) Alterations in NMDAR-mediated signaling within the laterodorsal tegmental nucleus are associated with prenatal nicotine exposure. *Neuropharmacology* 158:107744.
- Purgianto A, Loweth JA, Miao JJ, Milovanovic M, Wolf ME (2016) Surface expression of GABAA receptors in the rat nucleus accumbens is increased in early but not late withdrawal from extended-access cocaine self-administration. *Brain Res* 1642:336–343.
- Reese AL, Kavalali ET (2015) Spontaneous neurotransmission signals through store-driven Ca(2+) transients to maintain synaptic homeostasis. *Elife* 4:e09262.
- Scheetz AJ, Nairn AC, Constantine-Paton M (2000) NMDA receptor-mediated control of protein synthesis at developing synapses. *Nat Neurosci* 3:211–216.
- Sesack SR, Grace AA (2010) Cortico-basal ganglia reward network: microcircuitry. *Neuropsychopharmacology* 35:27–47.
- Snell LD, Nunley KR, Lickteig RL, Browning MD, Tabakoff B, Hoffman PL (1996) Regional and subunit specific changes in NMDA receptor mRNA and immunoreactivity in mouse brain following chronic ethanol ingestion. *Brain Res Mol Brain Res* 40:71–78.
- Stefanik MT, Milovanovic M, Werner CT, Spainhour JC, Wolf ME (2018) Withdrawal from cocaine self-administration alters the regulation of protein translation in the nucleus accumbens. *Biol Psychiatry* 84:223–232.
- Stroebel D, Casado M, Paoletti P (2018) Triheteromeric NMDA receptors: from structure to synaptic physiology. *Curr Opin Physiol* 2:1–12.
- Stutzmann GE, LaFerla FM, Parker I (2003) Ca²⁺ signaling in mouse cortical neurons studied by two-photon imaging and photoreleased inositol triphosphate. *J Neurosci* 23:758–765.
- Tang W, Wesley M, Freeman WM, Liang B, Hemby SE (2004) Alterations in ionotropic glutamate receptor subunits during binge cocaine self-administration and withdrawal in rats. *J Neurochem* 89:1021–1033.
- Tezuka T, Umemori H, Akiyama T, Nakanishi S, Yamamoto T (1999) PSD-95 promotes Fyn-mediated tyrosine phosphorylation of the N-methyl-D-aspartate receptor subunit NR2A. *Proc Natl Acad Sci USA* 96:435–440.
- Wang J, Ishikawa M, Yang Y, Otaka M, Kim JY, Gardner GR, Stefanik MT, Milovanovic M, Huang YH, Heng Y, Wolf ME, Schluter OM, Dong Y (2018) Cascades of homeostatic dysregulation promote incubation of cocaine craving. *J Neurosci* 38:4316–4328.
- Wang Y, Rao W, Zhang C, Zhang C, Liu MD, Han F, Yao LB, Han H, Luo P, Su N, Fei Z (2015) Scaffolding protein Homer1a protects against NMDA-induced neuronal injury. *Cell Death Dis* 6:e1843.
- Wee KS, Tan FC, Cheong YP, Khanna S, Low CM (2016) Ontogenic profile and synaptic distribution of GluN3 proteins in the rat brain and hippocampal neurons. *Neurochem Res* 41:290–297.
- Wee KS, Zhang Y, Khanna S, Low CM (2008) Immunolocalization of NMDA receptor subunit NR3B in selected structures in the rat forebrain, cerebellum, and lumbar spinal cord. *J Comp Neurol* 509:118–135.
- Werner CT, Stefanik MT, Milovanovic M, Caccamise A, Wolf ME (2018) Protein translation in the nucleus accumbens is dysregulated during cocaine withdrawal and required for expression of incubation of cocaine craving. *J Neurosci* 38:2683–2697.
- Wolf ME (2016) Synaptic mechanisms underlying persistent cocaine craving. *Nat Rev Neurosci* 17:351–365.
- Wolf ME, Tseng KY (2012) Calcium-permeable AMPA receptors in the VTA and nucleus accumbens after cocaine exposure: when, how, and why? *Front Mol Neurosci* 5:72.
- Wong HK, Liu XB, Matos MF, Chan SF, Perez-Otano I, Boysen M, Cui J, Nakanishi N, Trimmer JS, Jones EG, Lipton SA, Sucher NJ (2002) Temporal and regional expression of NMDA receptor subunit NR3A in the mammalian brain. *J Comp Neurol* 450:303–317.
- Wright WJ, Graziane NM, Neumann PA, Hamilton PJ, Cates HM, Fuerst L, Spenceley A, MacKinnon-Booth N, Iyer K, Huang YH, Shaham Y, Schluter OM, Nestler EJ, Dong Y (2020) Silent synapses dictate cocaine memory destabilization and reconsolidation. *Nat Neurosci* 23:32–46.
- Yang J, Jiang Q, Yu X, Xu T, Wang Y, Deng J, Liu Y, Chen Y (2020) STK24 modulates excitatory synaptic transmission in epileptic hippocampal neurons. *CNS Neurosci Ther* 26:851–861.
- Yuan T, Bellone C (2013) Glutamatergic receptors at developing synapses: the role of GluN3A-containing NMDA receptors and GluA2-lacking AMPA receptors. *Eur J Pharmacol* 719:107–111.
- Yuan T, Mameli M, O'Connor EC, Dey PN, Verpelli C, Sala C, Perez-Otano I, Lüscher C, Bellone C (2013) Expression of cocaine-evoked synaptic plasticity by GluN3A-containing NMDA receptors. *Neuron* 80:1025–1038.